YAW DYNAMICS CONTROL OF THREE WHEELED HYBRID VEHICLE BY TORQUE VECTORING

ÜÇ TEKERLİ HİBRİT ARACIN TORK AKTARIMI İLE DOĞRULTU KONTROLÜ

AHMET TARHAN

ASSOC. PROF. DR. S. ÇAĞLAR BAŞLAMIŞLI

Supervisor

Submitted to

Graduate School of Science and Engineering of Hacettepe University

as a Partial Fulfillment to the Requirements

for the Award of the Degree of Master

In Mechanical Engineering

2021

ÖZET

ÜÇ TEKERLEKLİ HİBRİT ARACIN TORK AKTARIMI İLE DOĞRULTU KONTROLÜ

AHMET TARHAN

Yüksek Lisans, Makina Mühendisliği Bölümü

Tez Danışmanı: Doc. Dr. Selahattin Çağlar BAŞLAMIŞLI

Ocak 2021, 77 Sayfa

Sunulan tez kapsamında üç tekerlekli hibrit aracın yanal dinamikleri incelenmiştir. Şasi, süspansiyon, direksiyon sistemi ve tekerlekler gibi mekanik ve hareketli parçalar Adams/Car yazılımında modellenmiştir. Diğer yandan İYM, elektrik motorları, şanzıman, batarya gibi güç üretme ve aktarma aksamı ile enerji yönetim sistemi, hız kontrolcüsü ve doğrultu kontrolcüsü MATLAB/Simulink yazılımı ile modellenmiştir. Enerji yönetim sistemi maksimum batarya stratejisi ile doğrultu kontrolcüsü ise LQR control stratejisi ile tasarlanmıştı. Ardından eş benzetim tekniği ile detaylı benzetim çalışmaları gerçekleştirilmiş ve araç hızının, ivmelenmenin, batarya seviyesinin, sürtünme katsayısının ve hibrit aracın mod değişimlerinden kaynaklanan tork transferinin yanal dinamiklere etkisi incelenmiş, bu etkiler altında doğrultu kontrolcüsünün performansı izlenmiştir.

Anahtar kelimeler: Tork Aktarımı, Hibrit Taşıt, Enerji Yönetim Sistemi, Üç Tekerlekli Araç, Çoklu Cisimler Dinamiği, Eş Benzetim

ABSTRACT

YAW DYNAMICS CONTROL OF THREE WHEELED HYBRID VEHICLE BY TORQUE VECTORING

AHMET TARHAN

Master of Science, Department of Mechanical Engineering

Supervisor: Assoc. Prof. Dr. Selahattin Çağlar BAŞLAMIŞLI

January 2021, 77 Pages

In this thesis, the lateral dynamics of the three-wheeled hybrid vehicle were evaluated. Mechanical components and moving parts such as the vehicle chassis, suspensions, steering system, and tires are modeled on Adams/Car software. On the other hand, powertrain components such as ICE, electric motors, generators, transmissions, batteries, and controllers such as Energy Management System, Speed Controller and Direct Yaw Controller are modeled in MATLAB/Simulink software. The energy management system is designed according to the maximum SoC strategy and the direct yaw controller with torque vectoring and active braking is designed according to the LQR control strategy. Then, detailed system analyses were performed with the co-simulation technique. The effects of speed, acceleration, battery level, friction coefficient and torque transfer resulting from mode change on lateral dynamics have been investigated and the performance of the yaw controller has been observed against these effects.

Keywords: Torque Vectoring, Hybrid Vehicle, Three Wheeled Vehicle, Multibody Dynamics, Co-simulation, Energy Management System

ACKNOWLEDGMENTS

I express my sincere appreciation to my supervisor Doç.Dr. Selahattin Çağlar BAŞLAMIŞLI for his valuable commands and helpfulness.

TABLE OF CONTENT

LIST OF FIGURES

LIST OF TABLES

SYMBOLS AND ABBREVIATIONS

Symbols

h_s	Height of sprung mass
ρ_a	Air density
A_f	Frontal area of vehicle
C_D	Drag coefficient
E_m	Battery Open Circuit Voltage
F_D	Drag force
F_x	Longitudinal tire force
F_y	Lateral tire force
J_w	Wheel's moment of inertia about its axis of rotation
M_z	Corrective Yaw Moment
R_D	Dynamic radius of wheel
V_m	Battery Voltage
f_r	Rolling resistance coefficient
k_{us}	Understeer coefficient
m_s	Vehicle sprung mass
δ_i	Inertial factor for rotating components
$\emptyset$	Roll angle
I	Vehicle Moment of inertia
u	Longitudinal velocity
δ	Steer angle
A	Current

M	Moment
P	Power
T	Torque
a	The distance between the vehicle center of mass and the front tire
b	The distance between the vehicle center of mass and the rear tire
c	Cornering stiffness
m	Vehicle mass
r	Yaw rate
v	Lateral velocity
w	Angular velocity of wheel
α	Tire lateral slip angle
η	Efficiency
θ	Grade
κ	Tire longitudinal slip angle

Abbreviations

ABS	Anti-lock Braking System
AWD	All-Wheel Drive
CoM	Center of Mass
DYC	Direct Yaw Controller
EMS	Energy Management System
ESC	Electronic Stability Control System
HEV	Hybrid Electric Vehicle
ICE	Internal Combustion Engine
IEA	International Energy Agency

PPS	Peak Power Supply
SAE	Society of Automotive Engineers
SoC	State of Charge
TV	Torque Vectoring
ZEV	Zero-Emission Vehicle

1. INTRODUCTION

Rapid urbanization has increased the number of vehicles used in cities and the demand for them is still growing. As a result, people faced some problems such as heavy traffic, parking problems, air pollution, and high transportation costs. Hence small, and fuel-efficient vehicles became more popular day by day. For this reason, three-wheeled vehicles with their small, light, and narrow design might take much more place in the feature of the automotive industry.

With regard to the new generation of city vehicles, studies are caried out not only on the form of the vehicle but also on the energy source. Nowadays, conventional vehicles which are powered with internal combustion engine are replaced by hybrid vehicles, so energy management system of hybrid vehicles are remarkable research topics. The origin of this work is a three-wheeled hybrid vehicle prototype developed in the Mechanical Engineering Department of Hacettepe University. The prototype vehicle is shown in Figure 1.

Figure 1: Three-wheeled Hybrid Vehicle Prototype.

Despite their advantages, three-wheeled vehicles have never achieved the popularity they deserve, due to the fact that, they tend to be unstable during the harsh lateral maneuver. Cambering or tilting system is recommended for enhancement in roll and lateral dynamics performance of three-wheeled vehicles and there are many studies in the literature on this subject [1] [2] [3] [4]. On the other hand, research about torque vectoring which is proven technology about increasing lateral dynamics performance of the vehicle, remains limited in particular three-wheeled vehicles. This is the first problem to be tried to solve in this work.

As stated before, the three-wheeled vehicle that is the subject of this study is powered by hybrid powertrains. Therefore, there is a necessity for an energy management system (EMS) that is responsible for deciding which energy source is used for traction according to the charge level of the battery and power demand. EMS operation can cause changes in the torque distribution between the rear and front axles, and if it occurs while turning, the lateral dynamic behavior of the vehicle may change, and some stability problems may arise. Effect of using hybrid drivetrain on lateral dynamics is the concern of our work. The purpose of torque vectoring or direct yaw-moment controller (DYC) is to enhance vehicle lateral dynamics performance and keeping the vehicle stable by redistributing torque among wheels. However, the energy management system also changes torque distribution with a different motivation. There might be some situations that energy management system and yaw controller conflict. Investigating the compatibility of these control systems is the last question that we will try to answer.

1.1. Research Aims

The aims of this thesis are:

- To obtain a detailed and non-linear model that can capture the dynamic behavior of the hybrid three-wheeled vehicle.
- To apply EMS and DYC on a three-wheeled vehicle.
- To investigate the performance of torque vectoring technology for a three-wheeled vehicle.
- To investigate the effect of torque transfer caused by EMS on lateral dynamics.

- To show that EMS and DYC are compatible.

1.2. Organization

In this study, the three-wheeled hybrid vehicle with DYC will be introduced. In the Literature Review chapter, basic information used in the study process, sources, and bases of the choices made are explained.

In the System Modeling chapter, details of the MSC Adams model of the vehicle will be illustrated. Then drivetrain of the vehicle and drivetrain components are explained, and sizing will be done for urban driving. Finally, modelling is accomplished after designing EMS and DYC. The next chapter System Evaluation is designated for investigating the performance of control system separately and together. To evaluate the EMS, US FTP-72 is going to be used as a drive cycle and longitudinal performance and fuel consumption results are obtained. Because no steering maneuver is included, DYC can not affect the analysis. In a similar way, to evaluate DYC, ramp input at a constant velocity and Iso Double Lane Change analysis will be performed without EMS. After each system are evaluated separately, final simulations are performed to investigate the behaviors of both systems together. By keeping steering constant, the vehicle is forced to follow varying speed-time drive cycles thus both systems will be enabled to be active.

2. LITERATURE REVIEW

2.1. Relevant Theory

2.1.1. Vehicle Dynamics Model

System simulation or control system design process begins with system modeling. It is required to contain a sufficient number of equations to capture system behavior accurately. However, the model needs to be simple enough to avoid excessive computational effort. Considering handling analysis, nonlinear system equations should cover four essential degrees of freedom which are longitudinal, lateral, yaw, and roll motions. In literature, there is a lot of research that sticks to the four DOF model by neglecting other motions such as pitch motion, suspension motion, body bounce, etc. [5] [6] [7] [8].In this thesis, a nonlinear vehicle is modeled in MSC Adams Car with 12 DOF, but four system equations will be derived to use for controller design.

2.1.1.1. Nonlinear Vehicle Model

The Newton's method is used to derive the system equations with respect to the Society of Automotive Engineers (SAE) coordinate system. In SAE coordinate system which is illustrated in Figure 2 ,is placed to the vehicle center of mass and the x axis is the axis located along the longitudinal axis of the vehicle in the positive direction when the vehicle is moving forward, together with y and z axes are contemplated right-handed to the x axis.

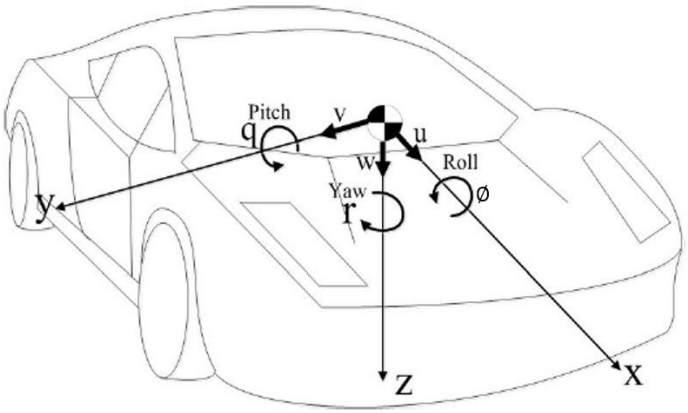

Figure 2: SAE Vehicle Coordinate System [9]

According to SAE coordinate system, yaw is a rotational velocity about the z-axis and defined as r, roll is the rotation around the x-axis and defined as $\emptyset$. Longitudinal speed is the vehicle speed in the x-axis and is defined as u and finally, lateral speed is the vehicle speed in the y axis and is defined as v.

Free body diagrams of the system with top view and rear view are shown in Figure 3 and Figure 4. During derivation, small angle assumption is made for roll angle.

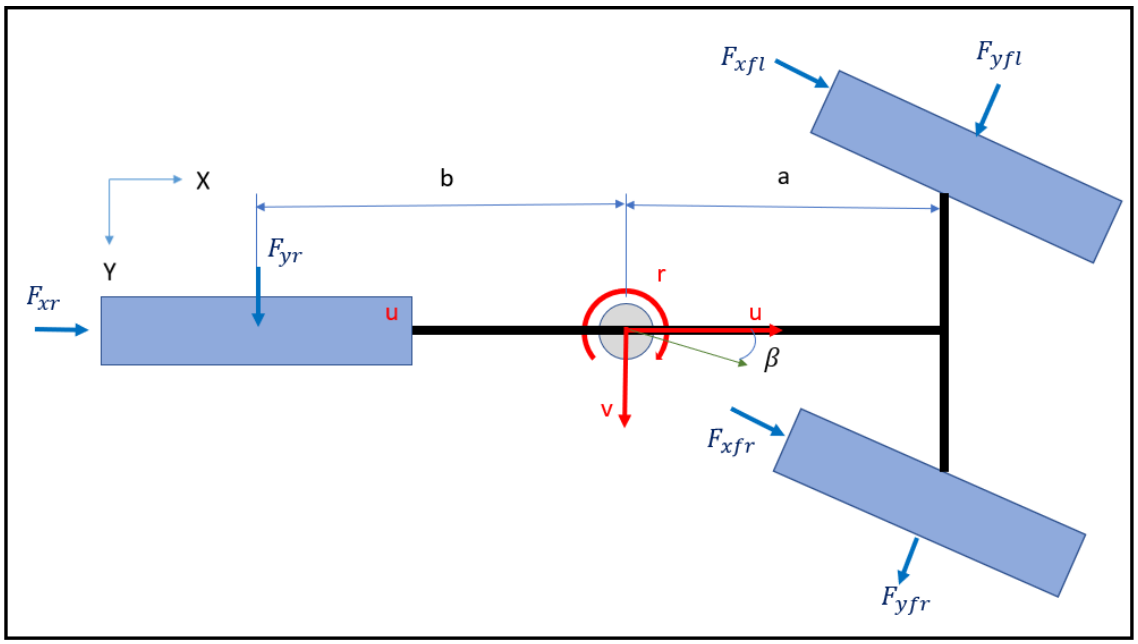

Figure 3: Free Body Diagram, Top View

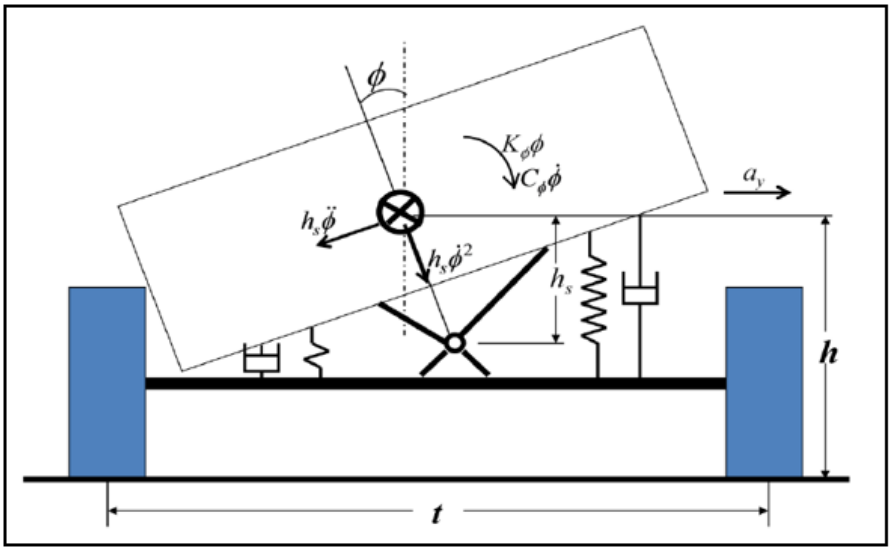

Figure 4: Free Body Diagram, Rear View

The force equilibrium in the x-direction for the vehicle body on is as follows

$$m(\dot{u} - vr) + 2m_s h_s r\dot{\emptyset} + \dot{r}h_s\dot{\emptyset} = \sum F_x \tag{1}$$

Where

$$\sum F_x = F_{xfl}\cos(\delta) - F_{yfl}\sin(\delta) + F_{xfr}\cos(\delta) - F_{yfr}\sin(\delta) + F_{xr} - 0.047C_D A_f u^2 \tag{2}$$

The force equilibrium in the y-direction for the vehicle body is as follows

$$m(\dot{v} + ur) + m_s(r^2 h_s\emptyset - (h_s\ddot{\emptyset} - h_s\dot{\emptyset}^2\emptyset)) = \Sigma F_y \tag{3}$$

Where

$$\sum F_y = F_{xfl}\sin(\delta) + F_{yfl}\cos(\delta) + F_{xfr}\sin(\delta) + F_{yfr}\cos(\delta) + F_{yr} \tag{4}$$

In this representation m and m_s are used to denote the mass and sprung mass of the vehicle, respectively. The distance between the vehicle center of gravity and the front tire is shown as a, and the distance between the center of gravity and the rear tire is shown b. F_{xi} and F_{yi} represent the tire longitudinal and lateral forces respectively with the

subscript i used for front left (fl), front right (fr), or rear (r), and δ is the steering angle of the front wheels. A_f and C_d represent the frontal area and the aerodynamic drag coefficient of the vehicle, respectively.

Equations for roll and yaw motions need to be uncoupled.

$$I_{zz}\dot{r} - I_{xz}\ddot{\emptyset} = \sum M_z \tag{5}$$

$$I_{xx}\ddot{\emptyset} - I_{xz}\dot{r} = \sum M_x \tag{6}$$

Above representation M and I are used to denoting moment and vehicle moment of inertia about the axis defined in subscript. After the necessary eliminations, expressions for yaw and roll motions are obtained as follows

$$\dot{r} = \frac{I_{xx}\sum M_z + I_{xz}\sum M_x}{I_{xx}I_{zz} - I_{xz}^2} \tag{7}$$

$$\ddot{\emptyset} = \frac{I_{xz}\sum M_z + I_{zz}\sum M_x}{I_{xx}I_{zz} - I_{xz}^2} \tag{8}$$

For vehicles that have symmetric mass distribution the product of inertia I_{xz} term became negligible value relative to I_{xx} and I_{zz}. After simplification

$$\begin{aligned} I_{zz}\dot{r} = \sum M_z = a\big(F_{xfl}\sin(\delta) + F_{yfl}\cos(\delta) + F_{xfr}\sin(\delta) + F_{yfr}\cos(\delta)\big) - bF_{yr} \\ + \frac{t}{2}\big(F_{xfl}\cos(\delta) - F_{yfl}\sin(\delta) - F_{xfr}\cos(\delta) + F_{yfr}\sin(\delta)\big) \end{aligned} \tag{9}$$

$$I_{xx}\ddot{\emptyset} = \sum M_x = m_s h_s(\dot{v} + ur) \; - \; m_s(r^2 h_s\emptyset \; - \; (h_s\ddot{\emptyset} - \; h_s\dot{\emptyset}^2\emptyset)) + M_{\emptyset} \tag{10}$$

Where

$$M_{\emptyset} = -K_{\emptyset}\emptyset - C_{\emptyset}\dot{\emptyset} \quad (11)$$

$K_{\emptyset}$ and C_{ϕ} are roll stiffness and damping, respectively.

2.1.1.2. Tire Forces and Friction Ellipse

Because vehicle behavior mostly depends on it, tire-road interaction forces have a crucial effect on vehicle dynamics simulation. There are several tire models in the literature to calculate the nonlinear response of a tire depends on slip angles. In this study The PAC2002 tire model which developed by MSC Software according to Tire and Vehicle Dynamics by Pacejka [10] is used.

Due to PAC2002 Tire Model's dynamics response is valid up to 12 Hz, it is suitable for handling and stability analysis such as steady-state cornering, lane change analysis, braking in turning, μ split braking, or ABS braking [11] .

The Magic Formula has capable of describing the behavior of a tire by producing a curve that passes through the origin and reaches a maximum and afterwards keep constant on a horizontal asymptote. The General form of the Magic Formula is given as

$$y(x) = Dsin[Carctan Bx - E(Bx - arctanBx)] \quad (12)$$

with

$$Y(X) = y(x) + S_V \quad (13)$$

$$x = X + S_H \quad (14)$$

where

Y is either F_x with X the longitudinal slip κ or F_y and X the lateral slip α.

B is stiffness factor, extends the curve

C is shape factor and effect on shape of curve

D is peak factor and decide the maximum value of curve

E is curvature factor effect on curve around maximum value, and location of peak.

S_V is vertical shift

S_H is horizontal shift

The output curve of the magic formula will be described in Figure 5 and the meaning of the curve parameters are indicated.

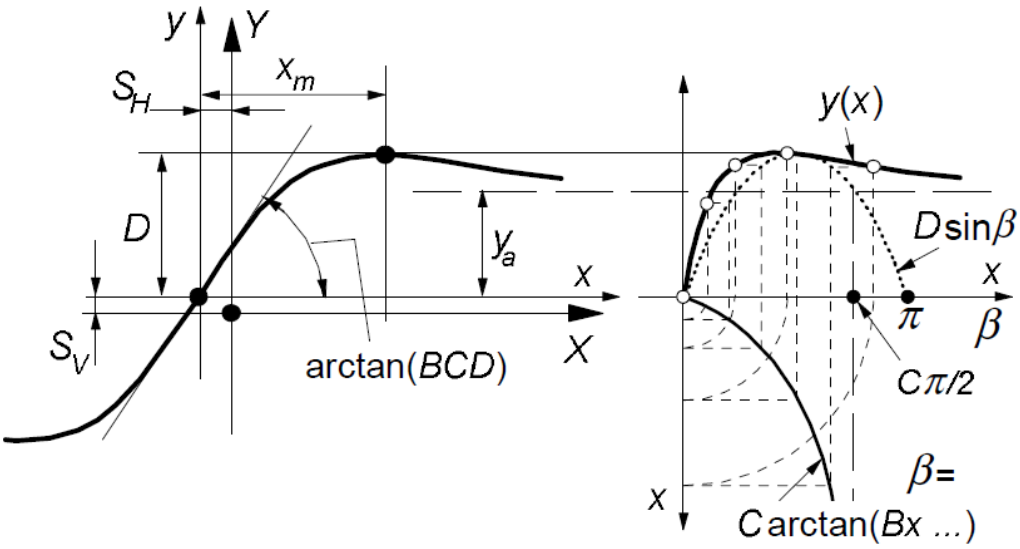

Figure 5: The Magic Formula Curve and Curve Parameters [10]

In the combined slip condition, the lateral force F_y decreases with the increasing F_x and vice versa because during motion maximum resultant reaction force between road and tire contact point is limited by friction ellipse. As it is seen in Figure 6, and also expressed in equation (15), increasing reaction force of tire up to beyond of friction ellipse result with saturation.

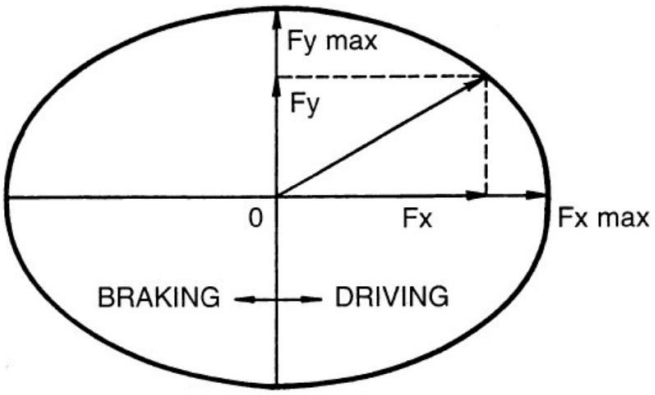

Figure 6: Friction Ellipse [12]

$$\frac{{F_x}^2}{{F_{x,max}}^2} + \frac{{F_y}^2}{{F_{y,max}}^2} \leq 1 \tag{15}$$

For a combined slip condition, F_x and F_y is calculated in Adams Car environment according to friction ellipse with the following expressions

$$\kappa_c = \kappa + S_{Hx} + \frac{S_{Vx}}{K_x} \tag{16}$$

$$\alpha_c = \alpha + S_{Hy} + \frac{S_{Vy}}{K_y} \tag{17}$$

K is the longitudinal stiffness of tire and subscript c means contact point.

$$\alpha^* = \sin(\alpha_c) \tag{18}$$

$$\beta = acos\left(\frac{|\kappa_c|}{\sqrt{K_c^2 + \alpha^*}}\right) \tag{19}$$

The following friction coefficients are defined

$$\mu_{x,act} = \frac{F_{x,0} - S_{Vx}}{F_z} \quad \& \quad \mu_{y,act} = \frac{F_{y,0} - S_{Vy}}{F_z} \tag{20}$$

$$\mu_{x,max} = \frac{D_x}{F_z} \quad \& \quad \mu_{y,max} = \frac{D_y}{F_z} \tag{21}$$

$$\mu_x = \frac{1}{\sqrt{\left(\frac{1}{\mu_{x,act}}\right)^2 + \left(\frac{\tan\beta}{\mu_{y,max}}\right)^2}} \quad \& \quad \mu_y = \frac{\tan\beta}{\sqrt{\left(\frac{1}{\mu_{x,max}}\right)^2 + \left(\frac{\tan\beta}{\mu_{y,act}}\right)^2}} \tag{22}$$

The forces after combined slip correction are

$$F_x = \frac{\mu_x}{\mu_{x,act}} F_{x,0} \quad \& \quad F_x = \frac{\mu_y}{\mu_{y,act}} F_{y,0} \tag{23}$$

2.1.1.3. Linear Bicycle Model

For the purpose of analyzing and designing DYC, vehicle dynamics modeling is the crucial step. It is required to build a model that represents lateral and yaw motion of three-wheeled vehicle sufficiently and could be linearized to reach an analytic solution with a reasonable effort. Therefore, the linear bicycle model which is shown in Figure 7 is used with the following assumptions.

- Tire deformations are always in linear region.
- The vehicle moves on flat surface.
- Traction/Brake forces are zero.
- Steering input and side sleep angles are very small.
- Lateral load transfer does not occur during cornering.
- Front wheels are lumped in single wheel at the centerline of the vehicle.
- Same steering angle is applied at front wheels.

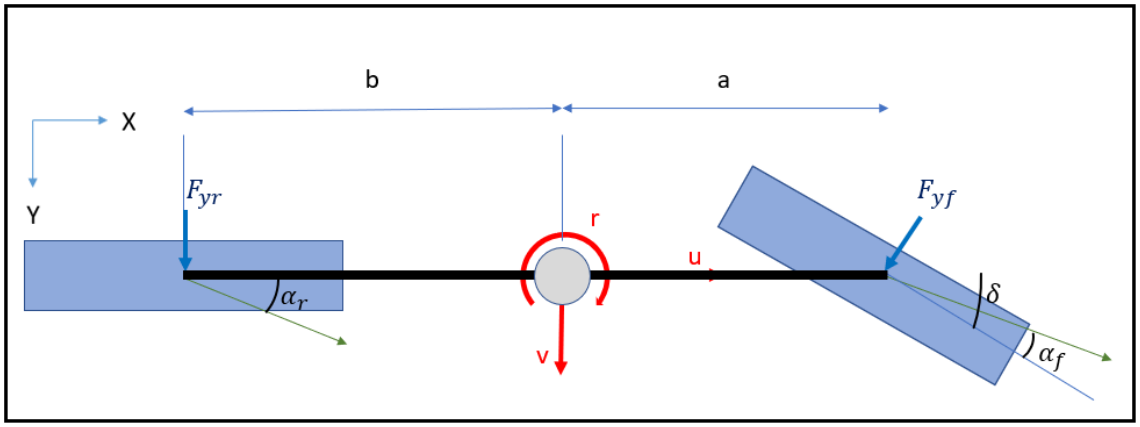

Figure 7: Linear Bicycle Model

According to Newton's 2nd Law, lateral and yaw motions could be expressed with the following equations.

$$m(\dot{v} + ur) = F_{yf}\cos(\delta) + F_{yr} + F_{xf}\sin(\delta) \tag{24}$$

$$I_{zz}\dot{r} = aF_{yf}\,cos(\delta) - bF_{yr} + F_{xf}sin(\delta) \tag{25}$$

In this representation m and I_{zz} are used to denote mass and moment of inertia of the vehicle about the Z-axis, respectively. The distance between the vehicle center of gravity and the front tire is shown as a, and the distance between the center of gravity and the rear tire is shown b. And u indicate longitudinal velocity of the vehicle. Because of the small steer assumption, these equations could be simplified to

$$m(\dot{v} + ur) = F_{yf} + F_{yr} \tag{26}$$

$$I_{zz}\dot{r} = aF_{yf} - bF_{yr} \tag{27}$$

Tire forces in the equations are the result of tire deflection and cornering stiffness. If c_f and c_r are cornering stiffness and α_f and α_r are slip angles for the front and rear axle respectively, lateral tire forces can be written in the following form

$$F_{yf} = c_f \alpha_f \quad \& \quad F_{yr} = c_r \alpha_r \tag{28}$$

Slip angles c_f and c_r can be written according to Figure 7 as

$$a_f = -\frac{v + ar}{u} + \delta \quad \& \quad a_r = -\frac{v - br}{u} \tag{29}$$

Inserting the above expressions into equations of motion we get

$$m(\dot{v} + ur) = -(c_f + c_r)\frac{v}{u} + (bc_r - ac_f)\frac{r}{u} + c_f \delta \tag{30}$$

$$I_{zz}\dot{r} = (bc_r - ac_f)\frac{v}{u} + (b^2 c_r - a^2 c_f)\frac{r}{u} + ac_f \delta \tag{31}$$

The above equations can be put into the general state space representation as follow

$$\dot{X} = AX + E\delta \tag{32}$$

Where

$$X = \begin{Bmatrix} v \\ r \end{Bmatrix}, \quad A = \begin{bmatrix} -\frac{c_f + c_r}{mu} & \frac{bc_r - ac_f}{mu} - u \\ \frac{bc_r - ac_f}{I_{zz}u} & -\frac{b^2 c_r + a^2 c_f}{I_{zz}u} \end{bmatrix}, \quad E = \begin{bmatrix} \frac{c_f}{m} \\ \frac{ac_f}{I_{zz}} \end{bmatrix}$$

Lateral velocity v and yaw rate r are state variables. On the other hand, steer input δ is the control input of the system.

2.2. Handling and Yaw Stability

Handling is a term for prescribing the relation between driver, vehicle, and environment during transportation. Vehicle handling qualities define the behavior of both vehicle and driver for all kinds of maneuvers under different environmental and road conditions. [13].

Therefore, it can be said that handling quality is the result of driver skills and vehicle handling performance. If vehicle response driver command fast and control of it is easy enough to decrease the necessity of driver skill, it can be concluded that the vehicle has good handling [14].

During turning, the vehicle should track the desired trajectory without displaying excessive understeer or oversteer behavior. In the understeer case, the vehicle could not produce enough yaw rate to follow the intended trajectory during turning therefore turning diameter of the vehicle becomes larger than intended. On the other hand, for an oversteer case, the vehicle tends to turn around the corner with the smaller diameter and might spin or became unstable eventually. Understeer and oversteer behaviors depict in Figure 8.

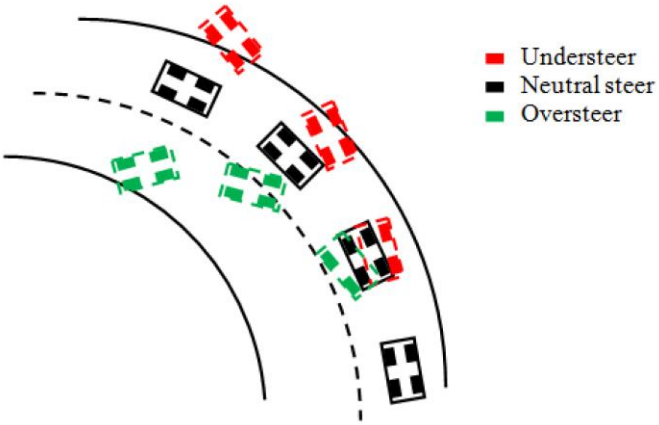

Figure 8: Handling Behavior during Steady State Cornering

In order to study handling behavior of vehicle during cornering, bicycle model can be used. From (32)transfer function between steer input and yaw rate can be derived as follow

$$r(s) = \frac{\frac{au^2m}{(a+b)c_r}s + u}{\frac{mIu^2}{(a+b)c_fc_r}s^2 + \frac{(c_f + c_r)Iu + mu(a^2c_f + b^2c_r)}{(a+b)c_fc_r}s + \frac{mu^2}{(a+b)c_fc_r}(bc_r - ac_f) + (a+b)}\delta \quad (33)$$

Negative eigenvalues indicate stability for equation(33) and it is possible only if the third term of the characteristic equation is positive because the first two terms are always positive

$$\frac{mu^2}{(a+b)c_fc_r}(bc_r - ac_f) + (a+b) > 0 \quad (34)$$

If:

- $bc_r - ac_f > 0$, then the vehicle is said to be **understeer,** and it is unconditionally stable.
- $bc_r - ac_f = 0$, then the vehicle is said to be **natural steer,** and it is unconditionally stable again.
- $bc_r - ac_f < 0$, then the vehicle is said to be **oversteer,** and it is unconditionally stable again.

To build stable system $bc_r - ac_f > 0$ condition must be satisfied. With this condition (34)could be rewritten as follow:

$$u^2k_{us} + (a+b) > 0 \quad (35)$$

In the above expression, k_{us} is called understeer coefficient and its value is an indication of handling behavior (See Figure 9). Generally, k_{us} is selected slightly positive to obtain a stable and responsive system.

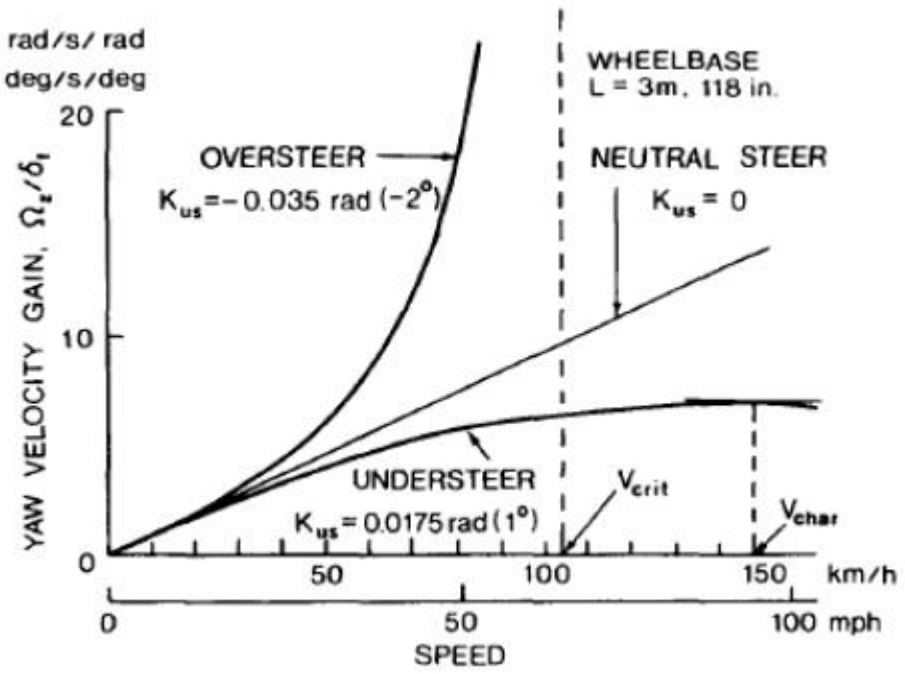

Figure 9: Yaw Velocity Gain vs Longitudinal Velocity [12]

2.3. Electronic Stability Control Systems

Electronic Stability Control Systems are the electronic systems that enhance lateral stability and handling quality of the vehicle automatically and used for helping the driver in dangerous situations caused by harsh maneuvers, slippery road conditions, or strong side winds. Ordinary driver's skills are limited in "linear range". In this range, change in lateral acceleration is proportional to given steering input, and also the lag time between driver input and vehicle response is short. Hence, adjusting heading is easy to control in that range [15] . However, with the increasing lateral acceleration, tire forces approach to saturation and yaw moment could not be generated by steering and lag time is became longer [16]. The driver that encounters that situation, tends to panic, and lose control because s/he is not used to drive in "nonlinear range".

ESC track vehicle states such as steering wheel angle, each wheel speed, lateral acceleration, and yaw rate by using sensors, and estimate intended yaw rate, and sideslip angle or lateral velocity according to reference vehicle at the same time. By comparing actual and desired states, ESC might produce corrective yaw moment thus establish yaw stability before nonlinear behaviors start. It is confirmed according to studies that are listed that ESC is very effective at preventing crushes.

- ESC would prevent 80 percent of skidding crashes and 35 percent of all vehicle fatalities [17]
- ESC would prevent 16.7 percent of all injury crashes, excluding rear-end collisions, and 21.6 percent of serious and fatal crashes [18]
- ESC would prevent 35 percent of single-vehicle crashes and 50 percent of fatal single-vehicle crashes. In addition, ESC would prevent 30 percent of head-on crashes and 40 percent of fatal head-on crashes [19]
- ESC would prevent 41 percent of single-vehicle crashes and 56 percent of fatal single-vehicle crashes [20]

ESC could be classified into 3 types: braking based, steering based, and torque vectoring. In this work braking-based stability control system and torque vectoring control system are going to be used.

In Figure 10, braking based ESC operation for an oversteer vehicle(a) and understeer vehicle(b) during left turning is illustrated. In this figure, ellipses that envelop each tire express the adhesion potential of that tire, and ellipses with dotted line express tires that reached saturation.

For an oversteer case, it is seen that the vehicle starts to spin because rear tires reach saturation and could not produce sufficient lateral force. At that moment, ESC intervenes by braking the front outside wheel and corrective yaw moment is produced. The secondary benefit of the braking front outside wheel is that the lateral force potential of that tire is decreased. As a result, vehicle heading is adjusted with the help of ESC.

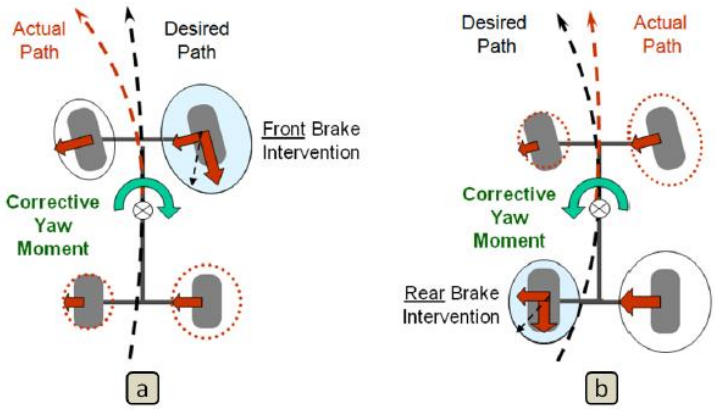

Figure 10: Braking-Based ESC System [21]

Contrary to oversteer condition, front tires reach their limit for the understeered vehicles. In this case, sufficient lateral force could not be produced from front tires to follow the desired trajectory. ESC brakes rear inner tire to produce corrective yaw moment and adjust heading.

Despite significant advantage of brake-based ESC on the stability of the vehicle in extreme maneuvers, it has one major drawback. Yaw moment generation by braking slows down the vehicle, therefore, decrease ride joy and fuel efficiency. The most promising solution to that is torque vectoring. Torque vectoring is the term that describes transferring driving or braking torque between axles or sides of a vehicle. Torque vectoring between axles changes tire potentials, hence handling characteristics can be change. For example, if applied torque is transferred from the front axle to the rear axle for the understeered vehicle, front wheels are able to generate more lateral force thus vehicle approach neutral steering. Conversely, traction torque should be transferred from rear to front to suppress oversteered behavior. On the other hand, applying torque unevenly between the left and right side generates yaw moment. In Figure 11, stability control with side-to-side torque vectoring is described. For the oversteered condition sufficient amount of torque is transferred from outer to inner wheel, and for the understeered condition, torque transfer is made from inner to outer to crate corrective yaw moment. Front wheels for understeer condition and rear wheels for understeer condition are selected for torque transfer, because of the fact that wheels on opposite axle reach saturation limit. Unfortunately, one wheel is placed at rear for three

wheeled vehicle, hence understeered condition could be corrected front to rear torque vectoring only.

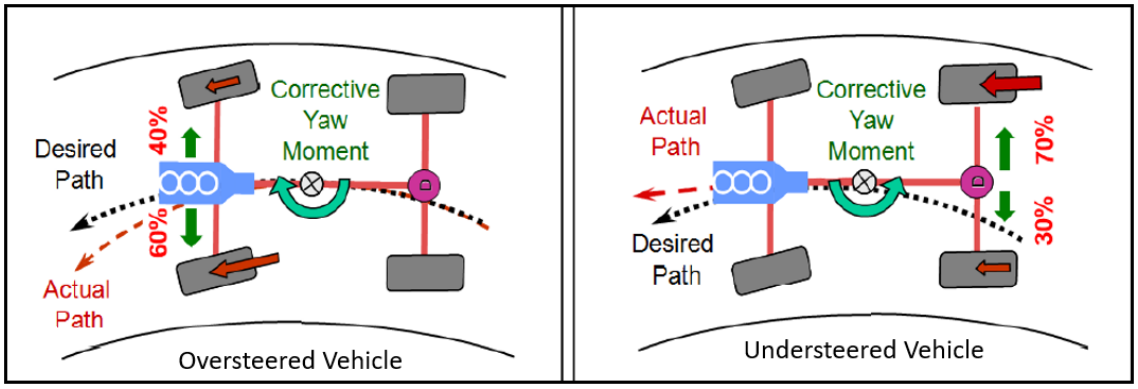

Figure 11: Stability Control with Torque Vectoring

Many studies show positive effects of torque vectoring on lateral stability and handling quality [22] [23]. For example, Ghoss et all. used torque vectoring on rear wheeled drive electric vehicle and obtained 10% improvement in understeer gradient of the vehicle and prevent spinning once vehicle tires exceed adhesion limit [24]. Saeedi & Kazemi studied the three-wheeled vehicle with torque vectoring control and find out vehicle remains stable during harsh maneuver thanks to torque vectoring [25]. Similar improvements are obtained for AWD vehicles according to study of Wheals et all [26] without loss in longitudinal performance and efficiency unlike brake-based ESC. Moreover, active braking is active only in an emergency and reported as disruptive by drivers. On the contrary, torque vectoring can be used constantly and almost every maneuver without disturbing the driver. However, it should be noted that driving torque is required for torque vectoring. If the driver releases the gas pedal or the amount of driving torque is limited, torque vectoring would not be sufficient. For such cases, brake-based ESC must intervene and establish lateral stability, or it can be said that torque vectoring and ESC should work together to reach full potential.

2.4. Hybrid Vehicle

According to International Energy Agency (IEA) road transportation is responsible for 17.9% of total CO2 emission in 2018 [27] and contribution of transportation to total

CO2 emission still growing. Despite their superior properties such as low CO2, CO and HC emission and high thermal efficiency, conventional diesel engines which are widely used in transportation could not be promising solution because of their high PM and NOx emissions. Diesel power vehicles are blamed for increase in NOx and air pollution in Europa [28], and several countries in European Union already introduce bans for them.

Electric vehicles seem the best solution to approach zero-emission vehicles (ZEV). Moreover, electric motors generate torque 10 to 100 times faster than the internal combustion engine or hydraulic braking system, and generated torque can be measured simultaneously with smaller uncertainty during driving. This enables to establish better feedback control systems on vehicle. Especially using separate motors on right and left wheels make easier and cheaper to apply stability torque vectoring [29]. However, some disadvantages of electric vehicles may prevent people from buying electric vehicles. These disadvantages due to inadequate energy source technologies including batteries, fuel cells, capacitors, and flywheels. Without advancing in technology, electric vehicles will not provide long driving range and short charging time with an affordable price. On the other hand, incorporating internal combustion engine (ICE) and electric motors, range of electric vehicle extend greatly and offer rapid refueling of liquid gasoline of Diesel. This configuration is called hybrid electric vehicle (HEV) and it requires only little change in driveline infrastructure. Another advantage of HEV is to increase the overall fuel efficiency of ICE and decrease pollutant emission because ICE operates only in its most efficient mode. By considering HEV is the combination of positive sides of conventional vehicles and electric vehicles, it is becoming a consensus that the HEV is not only an interim solution for the implementation of zero-emission vehicles but also a practical solution for the commercialization of super-ultra-low-emission vehicles [30].

2.4.1. HEV Drivetrain Architecture

In this chapter, HEV drivetrain architecture is classified into four as follows.

- Parallel HEV

- Series HEV
- Series-Parallel HEV
- Complex HEV

2.4.1.1. Series Hybrid Electric Drivetrain

In the series hybrid electric drivetrain configuration depicted in Figure 12-a, the vehicle is propelled with the only electric motor. The aim of the internal combustion engine in this configuration is to produce electricity via a generator. The generated electricity either charge the battery or directly used for generating traction by the electric motor. Series hybrid electric drivetrain offer several advantages:

- Due to there is no mechanical connection between the engine and drive wheels, ICE could be operated always within the maximum efficiency region. Besides, it is possible to use incompatible power sources in drive train thanks to mechanical decoupling such as high-speed engines like gas turbine or power plants that have a slow dynamic response like Stirling engines.
- Because of the fact that electric motor's torque-rpm profile could be ideal for traction, transmission would be unnecessary with proper motor selection. Furthermore, using multiple motors for each driven wheel makes differential redundant, as a result drivetrain could be much more simpler.

Despite of advantages, series hybrid electric drive train have some disadvantages, such as following.

- Two stage energy conversion between ICE and driven wheels cause inefficiency.
- The generator increases weigh and cost.
- Greater size is required for electric motor to match performance requirements in terms of acceleration and grading.

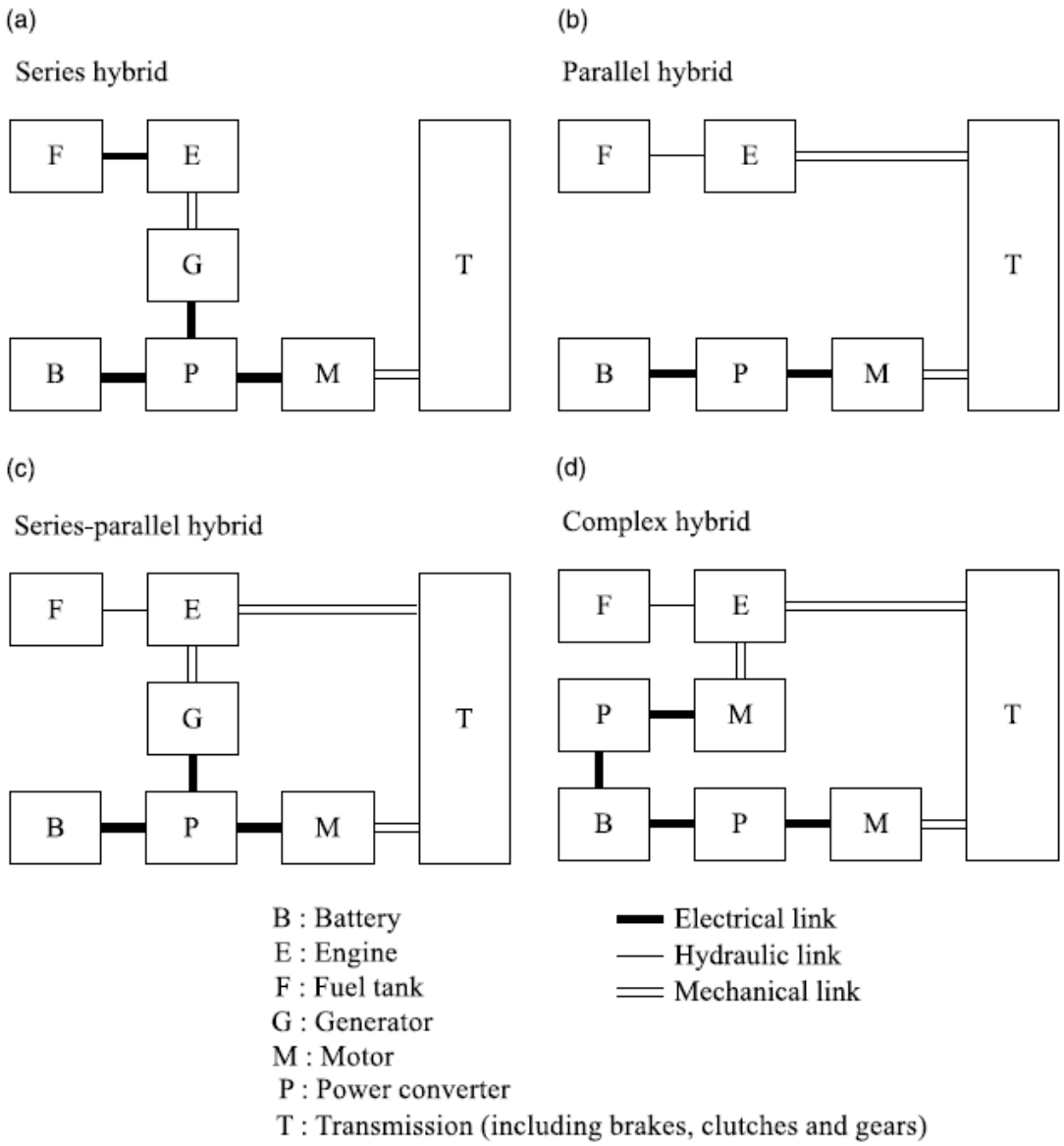

Figure 12: Classification of HE Drivetrains

2.4.1.2. Parallel Hybrid Electric Vehicle Drivetrain

In parallel hybrid electric vehicle drivetrain configuration which is depicted in Figure 12-b ICE and electric motor are mechanically coupled with two separate clutches and connected to the driveshaft. The Prime mover is ICE, and the duty of the electric motor is assisting ICE. Superiors of parallel hybrid electric drivetrain over series hybrid electric vehicle could be listed as below

- Both source of energy directly connected to the drive wheels therefore there is not loss because of additional energy conversion.

- The generator is not necessary and electric motors may be smaller.

The main disadvantage of parallel hybrid electric drivetrain is that using multi-gear transmission is necessary at between driven wheel and ICE.

2.4.1.3. Series-Parallel Hybrid Electric Drivetrain

Series parallel hybrid electric drivetrain which is depicted in Figure 12-c, uses combine advantages of both parallel and series configurations by adding mechanical coupling between driveshaft and electric motor to series hybrid configuration. It offers an increase in fuel efficiency with more initial cost.

2.4.1.4. Complex Drivetrain

In this configuration, the motor and engine are connected to each other with a planetary gear set. Therefore, the electric motor could be used as a traction motor or generator.

3. SYSTEM MODELING

3.1. Introduction

Successful application of control theory starts with proper system modelling. Investigation of Yaw Stability System and Energy Management System for a tadpole designed three wheeled vehicles, which tends to be unstable naturally, requires detailed modelling. Because of large displacements and highly nonlinear external forces, multibody dynamics method provides fast and reliable solution for vehicle dynamics problem. But It loses advantages in terms of function-based modelling and control system design against block diagram modelling.

In this work, to combine the advantages of the multibody dynamics method and block diagram system modeling, two software, Adams Car and MATLAB/Simulink, are used together. This chapter explains modeling details for both methods and software.

3.1.1. Modeling Layout

Mechanical components and moving parts such as the vehicle chassis, suspensions, steering system and tires are modeled on Adams Car. On the other hand, powertrain components such as ICE, electric motors, transmissions, batteries, and controllers such as Energy Management System, Speed Controller and Direct Yaw Controller are modeled in MATLAB / Simulink. Modelling composition is described in Figure 13.

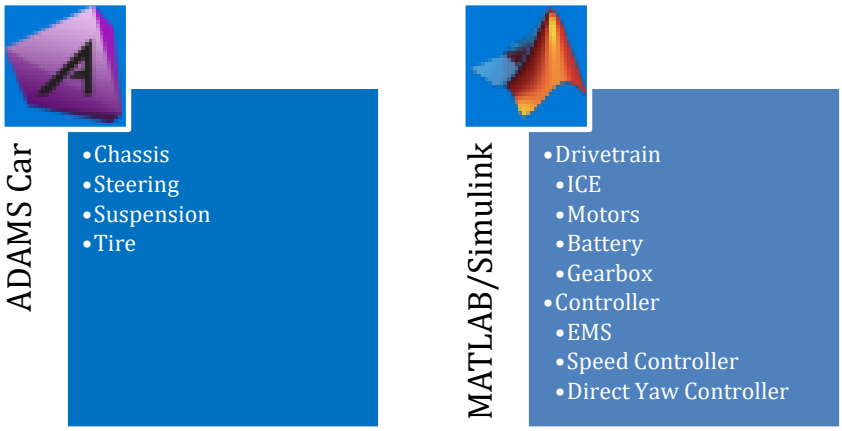

Figure 13 Modelling Layout - I

Co-simulation technique provides the capability for run time coupling of Adams/Car and Matlab Simulink models. Softwares run one by one and pass the required information to each other. In this study, Adams model takes differential torque for each wheel and predefined time-dependent steer data as an input and calculates vehicle dynamic behavior. Then pass vehicle dynamic information which is required for controllers such as wheels speed, longitudinal velocity, and yaw rate to Simulink model. Simulink model takes Adams/Car output and calculates differential torques according to time-dependent velocity data. Data transformation sequence illustrated in Figure 14. Details of velocity and steer input are explained in System Evaluation chapter.

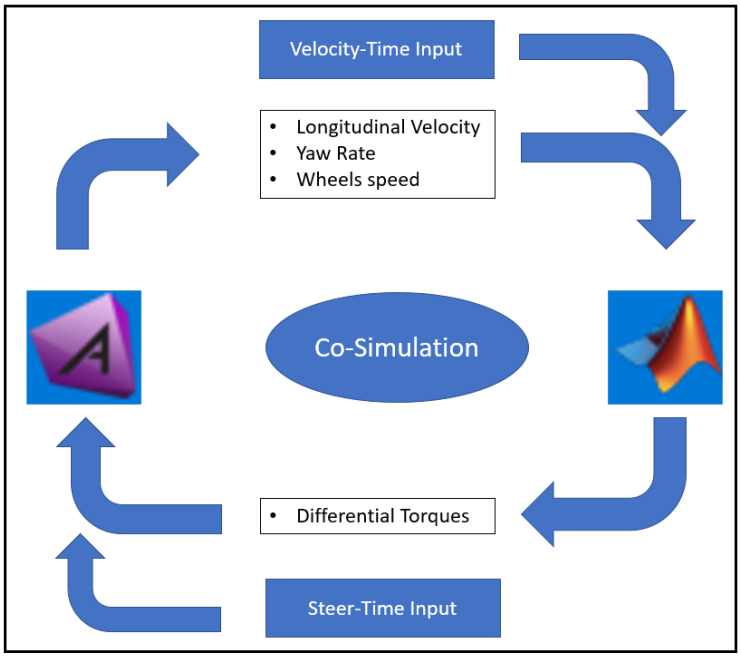

Figure 14: Modelling Layout – II

3.1.2. Chassis Layout

Figure 15: Chassis Layout depicts the layout of vehicle. As shown in Figure 15 the vehicle composed of two front tires and one rear tire, that kind of configuration is also known as tadpole design. Front tires are powered by two electric motors and the source of power for rear tire is internal combustion engine (ICE) therefore, in terms of HEV drivetrain architecture, vehicle layout could be expressed as parallel hybrid configuration. Because

ICE and electric motor are not placed sequentially, and they provide mechanical power to vehicle separately.

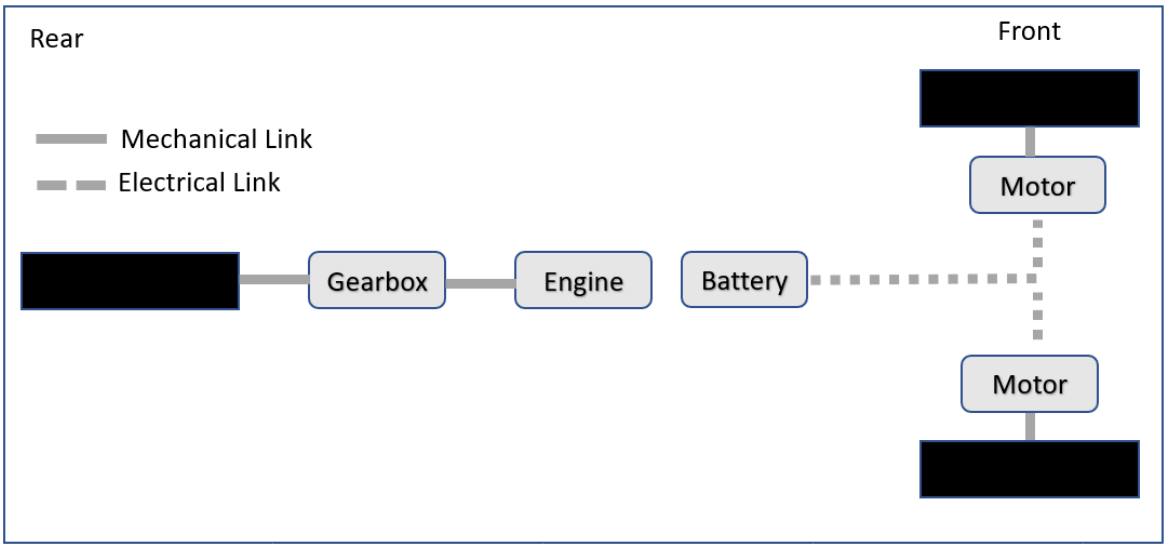

Figure 15: Chassis Layout

3.2. Three Wheeled Vehicle Modelling with Multi Body Dynamics

Adams/Car shows better performance for capturing the dynamic behavior of highly nonlinear problems such as large displacement and contact interactions. Thus, mechanical components chassis, suspension, steering system, and tires are modeled in Adams/Car. Isometric view of the Adams/Car model shown in Figure 16.

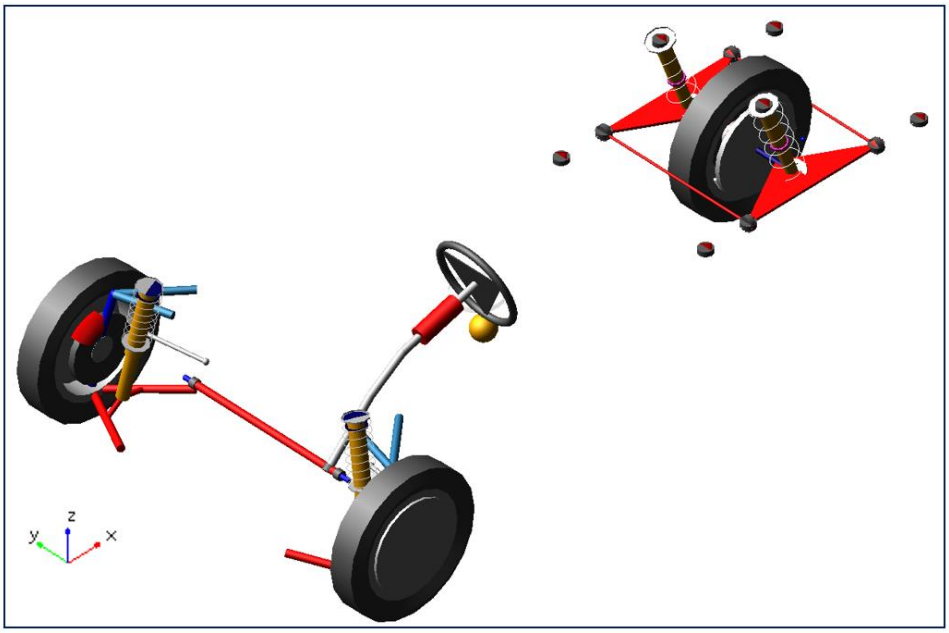

Figure 16: Full View of Adams Car Model

Table 1 depicts the location and orientation of the local coordinate system of vehicle assembly with respect to the global coordinate system. Mass and Inertia tensor is written with respect to the local coordinate system of the vehicle in this table.

Table 1: Mass Properties of Vehicle Assembly

	X	Y	Z
CoM Location[mm]	1505	0	300
Orientation[deg]	0	0	0
Mass[kg]	606		
I_{xx}[kgm^2]	150		
I_{yy}[kgm^2]	500		
I_{zz}[kgm^2]	500		

The operating environment is also modeled in Adams/car. In this study, it is assumed that the road is perfectly flat, rigid and friction is constant everywhere. Also, wind forces are ignored except for drag force which is caused by vehicle velocity. Drag force is calculated with the following expression [31]

$$F_D = \frac{1}{2}\rho_a C_D A_f V^2 \tag{36}$$

Where, ρ_a is air density, A_f is front area, C_D is aerodynamic drag coefficient, and V is the velocity of vehicle. During simulation, calculated drag force is applied on vehicle chassis part in opposite direction of velocity. Assumed values of operation environment is given in

Table 2: Operating Environment Parameters

A_f	1.5 m^2
C_D	0.3
ρ_a	1.205 kg/m^2

The following sections, details of front and rear suspensions and tires will be discussed.

3.2.1. Front Suspension

Double wishbone suspension template from Adams/Car library is directly used in the model. In this template, all subsystem is modeled with kinematic constraints. Lower and upper control arms connected to the chassis with a revolute joint. The connection between control arms and kingpin are made by spherical joints. And the revolute joint is used again for the connection between spindle and kingpin. Differential torque for each wheel is applied at right and left spindles directly. Figure 17 depicts left side of the front suspension.

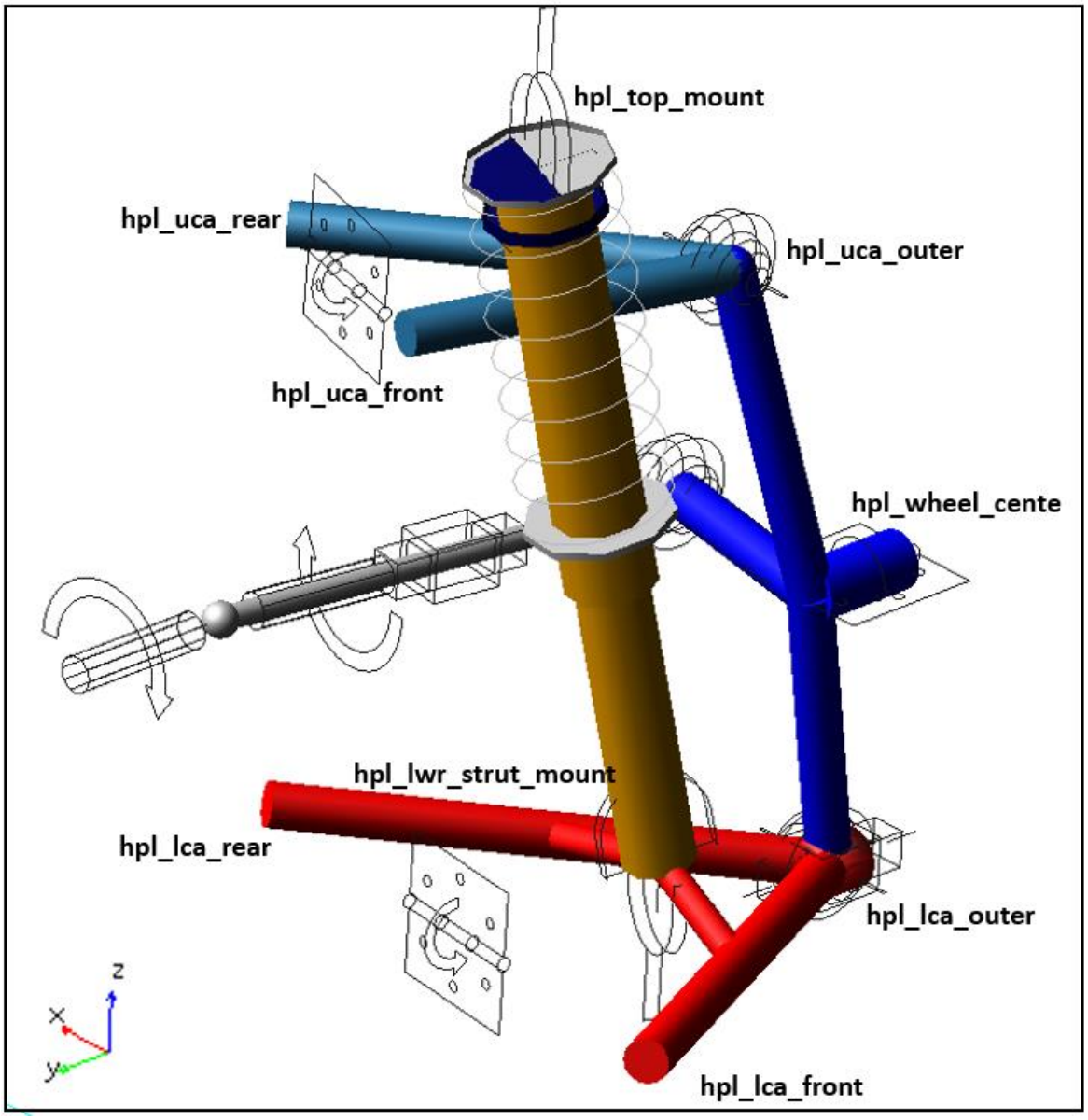

Figure 17: Front Suspension

The hardpoint locations of the left side of the front suspension are given in Table 3. Right, and left sides are completely symmetrical with respect to the XZ plane.

Table 3: Front Suspension Hard Point Locations

	X[mm]	Y[mm]	Z[mm]
hpl_lca_rear	567	-450	195
hpl_lca_front	167	-400	190
hpl_lwr_strut_mount	367	-600	190
hpl_lca_outer	367	-750	140
hpl_wheel_cente	367	-760	340
hpl_uca_front	467	-450	565
hpl_uca_outer	407	-675	565
hpl_uca_rear	617	-490	570
hpl_top_mount	407	-500	690

Spring reaction force behavior with respect to displacement of strut is assumed linear, and spring stiffens is chosen as 125 N/mm. On the other hand, damper reaction force behavior with respect to the strut velocity is given in Figure 18

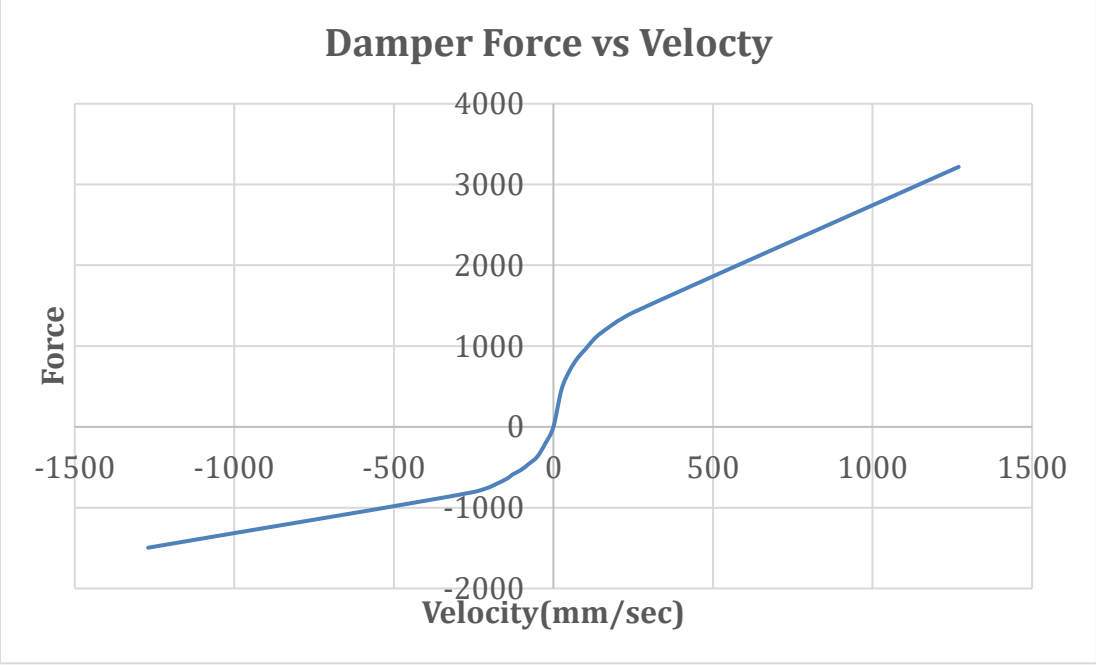

Figure 18: Damper Force vs Velocity

Camber and toe angels set to zero for front suspension.

3.2.1.1. Rear Suspension

There is not any available template for the rear suspension of the three-wheeled vehicle in Adams/Car library, therefore it must be built from stretch.

Rear suspension subsystem, composed of trailing arm, spindle, strut, and fixing rods as shown in Figure 19: View of Rear Suspension. Adams/Car is designed for 4 wheeled vehicles; therefore, it is required to model some part of the suspension as right and left like trailing arm. In this model there are two trailing arms indeed, but to force left and right parts move together, they tied up with fixing rod. To avoid redundant kinematic constraints, highly stiff bush elements are used for connection. Bushes at point hp[r/l]_subframe_front, hp[r/l]_strut_lwr_mount, hp[r/l]_top_mount, have high stiffness(1e5 N/mm) and damping coefficient(1e5 N/mm-sec) for all direction except for rotation about Y axis, as a result trailing arm and wheel can rotate about an axis which pass through hpl_subframe_front and hpr_subframe_front points, relative to vehicle chassis.

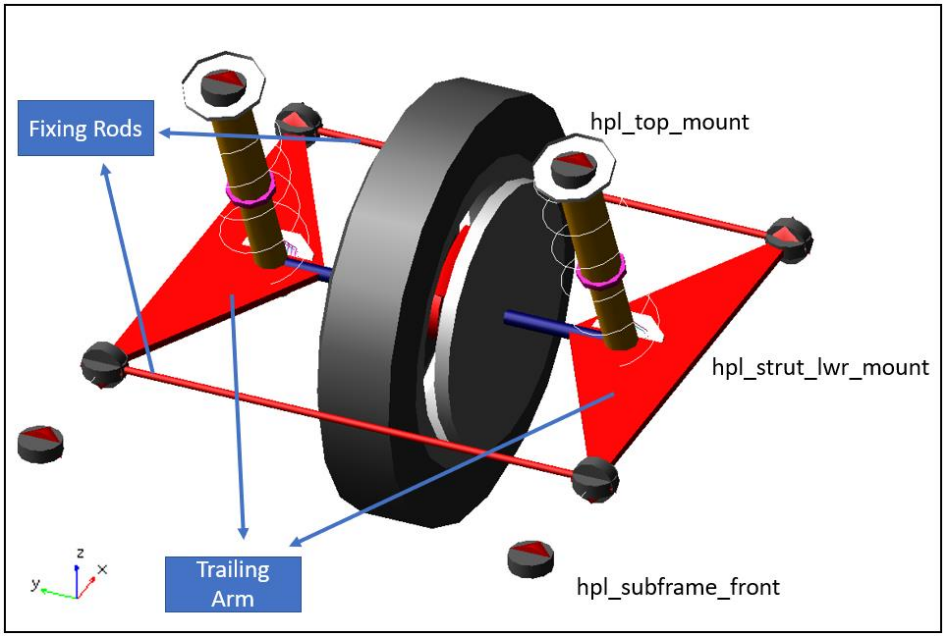

Figure 19: View of Rear Suspension

Same spring and damper properties are same for rear suspension with front suspension.

Harp point location of the left side of rear suspension is given in Table 4. Right and left sides are completely symmetrical with respect to XZ plane.

Table 4: Rear Suspension Hard Point Locations

	X[mm]	Y[mm]	Z[mm]
hpl_subframe_front	2183	-350	340
hpl_top_mount	2683	-250	340
hpl_strut_lwr_mount	2558	-250	690

3.2.2. Tire Modeling

Adams/Car provides several tire types for different analysis requirements. Because of the fact that the handling performance of the vehicle is investigated in this study, Pacejka tire modeling is used. The coefficients that are required for Pacejka modelling is given in APPENDIX A.

Mass properties of wheels is given in Table 5. Note that inertia tensor is written according to wheel local coordinate system.

Table 5: Mass Properties of Tires

	Front	Rear
Mass[kg]	25	30
I_{xx} & I_{yy} [kgmm^2]	8.0E+05	9.6E+05
I_{zz} [kgmm^2]	1.0E+06	1.2E+06

3.3. Drivetrain Modeling with Block Diagrams

The configuration of the drivetrain for the three-wheeled vehicle is determined as a parallel hybrid configuration. Therefore, component selection and sizing strategy is based on el power peaking strategy [32] . In this strategy, engine supply the power needed

during cruise on a flat road or a mild grade or mean power during stop and go driving pattern, while electric motor with battery supplies the power to meet the load at peak.

3.3.1. Internal Combustion Engine

ICE should be capable of supplying enough power to vehicle during transportation with constant speed on both a flat road and mild grade road without help of electric motor. For such requirement, needed power could be calculated with the following expression [33].

$$P_e = \frac{V}{1000\eta_{t,e}}\left(Mgf_r + \frac{1}{2}\rho_a C_D A_f V^2 + Mgi\right) \tag{37}$$

According to Equation (37), capacity of an engine of a three wheeled vehicle with the following parameters, rolling resistance coefficient $f_r = 0.01$, transmission efficiency $\eta_{t,e} = 0.9$ and road grade $i = \%5$, should be around 11.6 kW to travel with $V = 90\ km/h$.

In this study ICE is derived from Geo Metro 1.0L(41 kW). Torque and fuel consumption mapped data with respect to engine speed are taken from the ADVISOR file FC_SI41_emis and scaled by 0.4 to reduce maximum power output of engine around 5000 rpm speed so that match power requirement (Figure 20). To model ICE in Simulink, Mapped SI Engine block from Power Train Block set is used. Mapped SI Engine block takes engine speed and desired torque as an input and calculate output torque and fuel consumption by using scaled torque-speed (Figure 21) and fuel consumption rate (Figure 22) data.

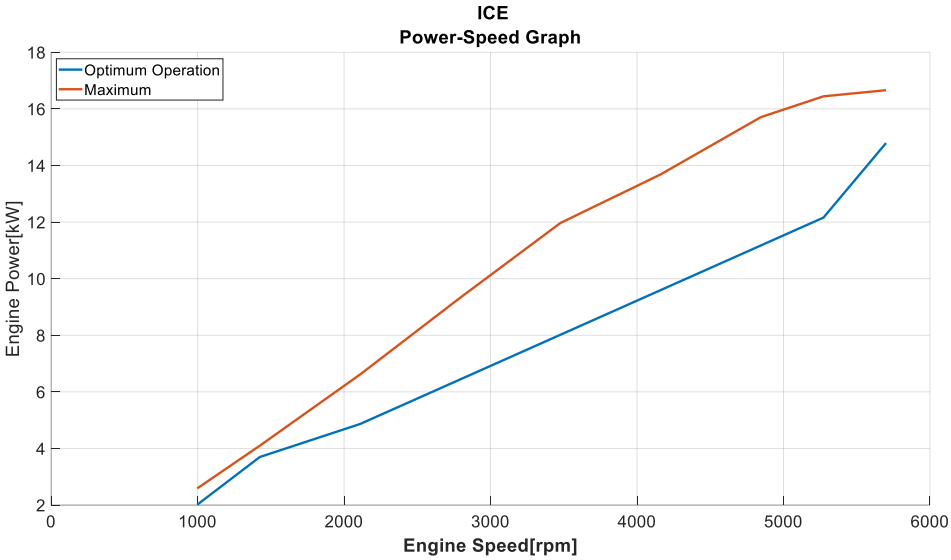

Figure 20: ICE Power-Speed Characteristics

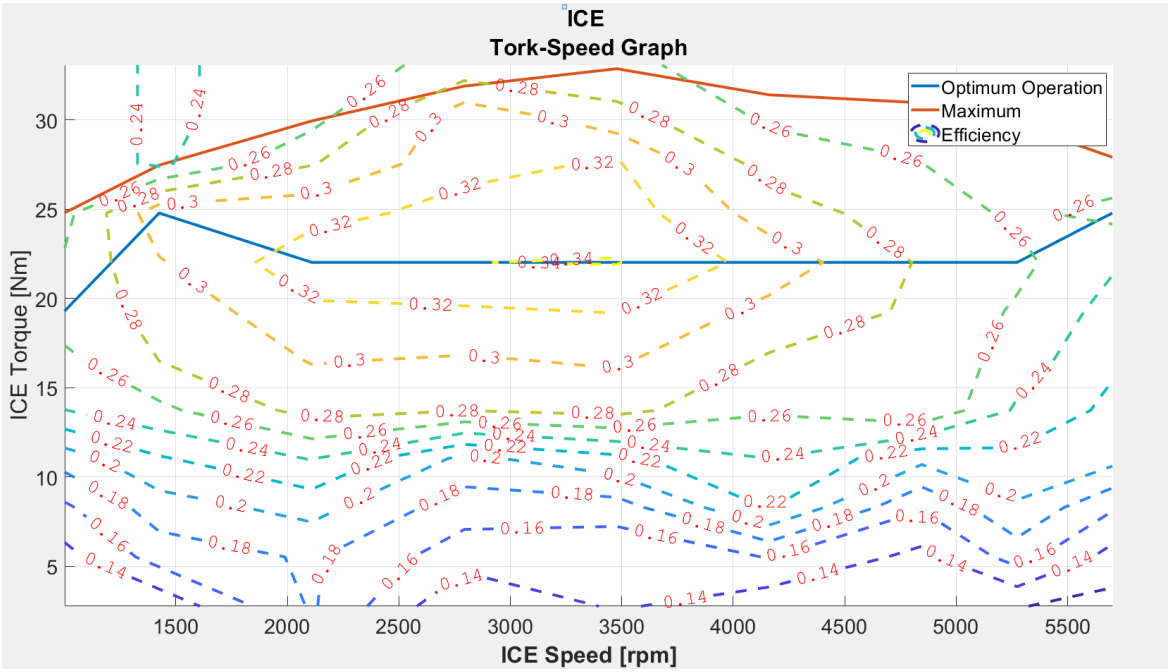

Figure 21: ICE Torque-Speed Characteristics

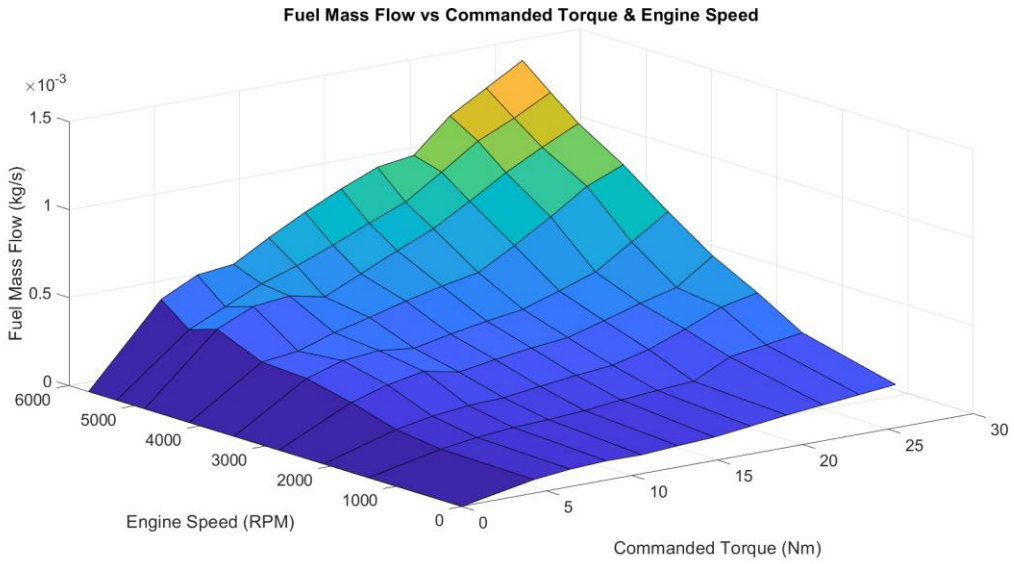

Figure 22: Fuel Consumption Rate

3.3.1. Transmission

Oscillation in torque demand during transportation mostly provided by electric motors and ICE perform its optimum thereby design strategy of transmission based on decreasing fuel consumption. During the simulation, gear selection is done according to vehicle speed. To do so, the transmission is modeled by using the lookup table. It takes vehicle speed as input and produces predefined gear ratio. The final drive is the gear between transmission and spindle. Therefore, the resultant gear ratio is the multiplicity of the final drive and related gear ratio.

Corresponding gear ratio and velocity values (Table 6), force ICE to run around its sweet spot which is located between 3200 and 4500 rpm.

Table 6: Transmission Gear Ratio

Gear	Gear Ratio	Velocity [km/h]
1	6.5	19
2	4.5	27
3	3.6	37.8
4	2.3	53.1
5	1.6	75
Final Drive	4	

3.3.1. Electric Motors

The main purpose of electric motors in a hybrid vehicle is to supply peak power to drive train. In other words, while ICE was producing power for steady-state loads such as rolling resistance or air drag, electric motors were supposed to handle dynamics loads like inertial loads in acceleration. With this initial assumption, it is possible to obtain the maximum electric motor power requirement as follow [34].

$$P_{m,max} = \frac{M\delta_i}{\pi t_f}\left(\frac{V_b^2 + V_f^2}{2}\right)(kW) \tag{38}$$

Where δ_i is the inertial factor for rotating components, M is the mass of vehicle, t_f is the acceleration time in second, V_b is the base speed of vehicle and V_f is the base speed of vehicle. Note that, this approach cause over estimation, because ICE might have excessive power to help acceleration and that excessive energy can be found following expression.

$$P_{e,a} = \frac{1}{t_a - t_i} \int_{t_i}^{t_a} (P_e - P_r) dt \quad (39)$$

Where P_e is the power of ICE and P_r is the resistance power. It should be noted that result of an equation (39) depends on road cycle and transmission gear ratios. Therefore, after several iteration with road cycle CYC_UDDS which is taken from ADVISOR, maximum required power is found for each motor as 5.85 kW. The maximum torque output of the corresponding motor according to motor speed and its efficiency map is illustrated in Figure 23.

In order to model Electric motor Mapped Motor Block from Power Train Block Set of MATLAB/Simulink is used. Mapped Motor Block takes battery voltage, motor speed and desired torque as an input and calculate output torque and current. Output current calculation is done with the following expression.

$$A_m = \frac{w_m T_m}{V_m}$$

Where A_m is the current, w_m is the motor speed, T_m is the motor output torque, and V_m is the battery voltage.

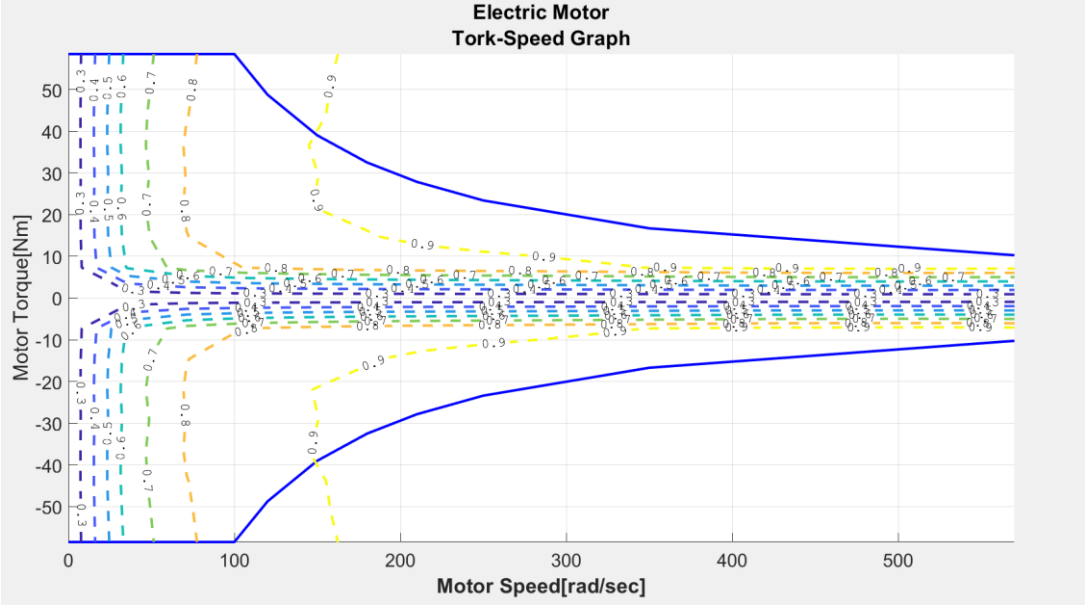

Figure 23: Motor Torque-Speed Characteristics

In case of regenerative braking same motor characteristic is used with negative sign convention.

3.3.2. Battery

The battery is modeled by using the Datasheet Battery block from the Power Train Block set of MATLAB/Simulink. Datasheet Battery block takes combined current that comes from electric motors as input and determines output voltage by using lookup tables for the battery open-circuit voltage (Figure 24) and internal resistance (Figure 25). The lookup tables are functions of state of charge (SoC).

To calculate the voltage, the block implements these equations.

$$E_m = f(SoC) \tag{40}$$

$$R_{int} = f(SoC) \tag{41}$$

$$V_T = E_m + I_{batt} R_{int} \tag{42}$$

$$I_{batt} = \frac{I_{in}}{N_p} \tag{43}$$

$$V_{out} = N_s V_T \tag{44}$$

$$SoC = \frac{1}{Cap_{batt}} \int_0^t I_{batt} dt \tag{45}$$

Where E_m is battery open-circuit voltage, I_{batt} is per module battery current, I_{in} in combined current from flowing from the battery network, R_{int} is battery internal resistance, N_s is number of cells in series, N_p is number of cell in parallel, V_{out} is the combined voltage of network, V_T per module battery voltage and Cap_{batt} is battery capacity.

Battery composed of 7 cells in series and 9 cells in parallel. Rated capacity is 0.5 Ah for each battery cells.

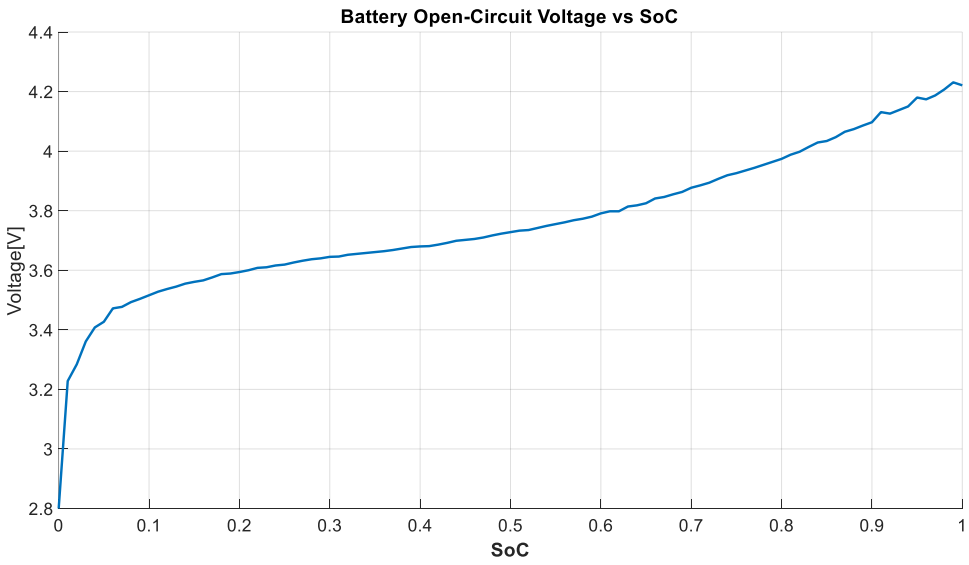

Figure 24: Per Module Battery Voltage

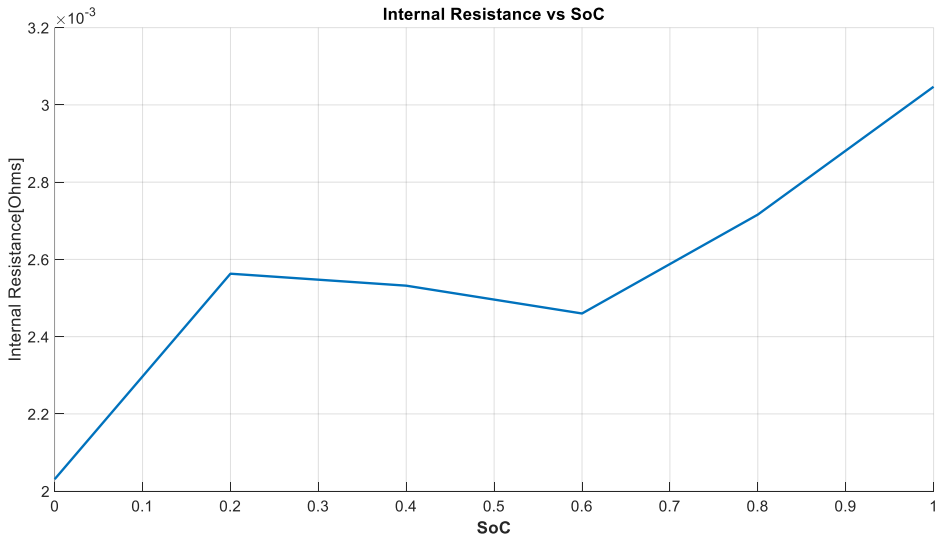

Figure 25: Per Module Battery Internal Resistance

3.4. Control System

3.4.1. Speed Controller

The Drive cycle that is going to be used to investigate EMS behavior is simply a lookup table that specifies vehicle longitudinal speed in time. Therefore, it is necessary to have a block that tracks the difference between vehicle speed and drive cycle output for that time instance and transform that information into torque demand to follow the drive cycle with sufficient performance. For this purpose, PID controller is used as a speed controller, shown in Figure 26. Controller gains are chosen manually using trial-and-error approach.

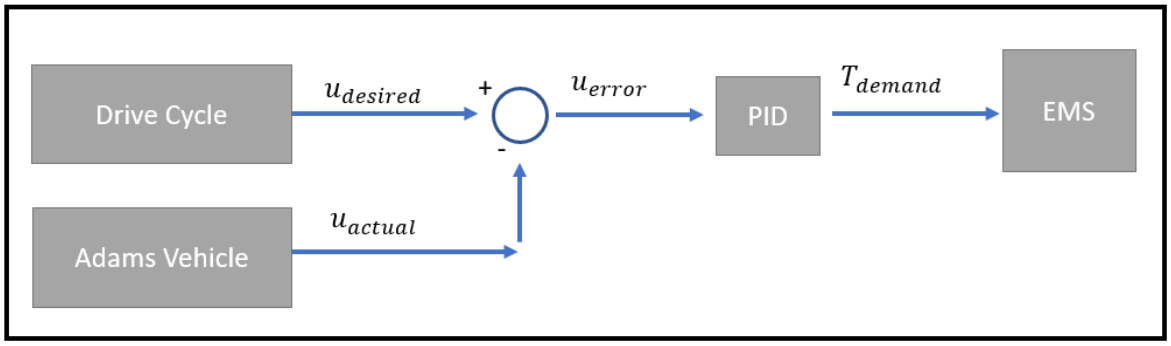

Figure 26: Speed Controller

3.4.2. Energy Management System

The energy management system is responsible for deciding how much energy is generated by ICE or electric motors during transportation. The decision is made according to driver demand and vehicle condition with proper energy management strategy. In hybrid vehicle applications, there are several energy management strategies to decrease fuel and emission consumption and they can be classified into two categories as rule-based strategies [35] and optimization-based strategies [36]. Optimization-based control strategies offer the best performance when the drive cycle is known. In addition, they have some disadvantages such as requiring complicated mathematical modeling and high computational effort. On the other hand, ruled based strategies widely used with their simplicity and low computational requirement even some deficit in overall performance.

By considering three-wheeled vehicles as a personal vehicle that is used for (mostly)city and urban driving without certain driving cycle and stop-and-go driving pattern, Maximum SOC Control Strategy is selected as a ruled based strategy for energy management system.

According to Maximum SOC Control Strategy, ICE is used as a prime mover for the vehicle, and charge battery if the engine efficiently produce power more than required at that time without exceeding full SoC value. In Figure 27 control strategy is described by plotting maximum power curves of different operating modes with respect to vehicle speed. Points A, B and C represent power demands in different conditions.

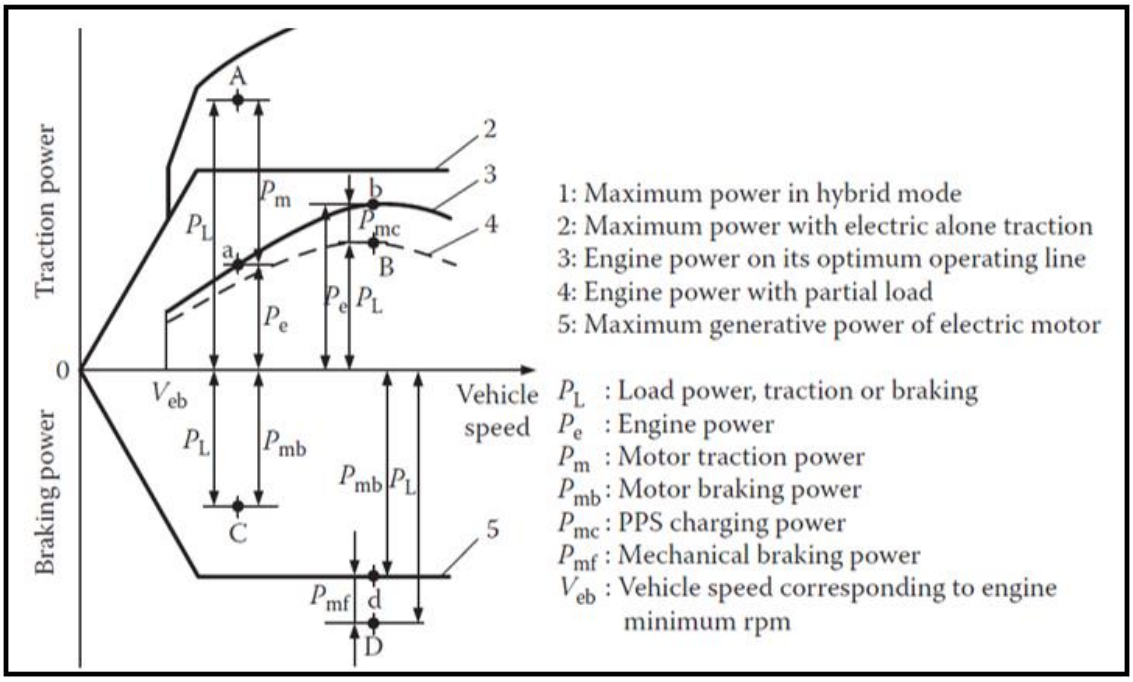

Figure 27: Operating Mode Based on Power Demand [33]

The operation modes are explained as follows.

Motor-alone propelling mode: To operate stable and considerably sufficient in term of low fuel consumption or carbon emission rate, the vehicle needs to reach a certain speed which is defined V_{eb}. In order to avoid those deficiency only electric motors operate below V_{eb}. At that state ICE is shut down or idles, as a result, the engine power, electric traction power, and PPS discharge power will be as follow

$$P_e = 0 \tag{46}$$

$$P_m = P_L \tag{47}$$

$$P_{pps\text{-}d} = \frac{P_m}{\eta_m} \tag{48}$$

Where; P_e is the engine output, P_L is the demanded power by driver for propelling, P_m is the power output of the electric motors, $P_{pps\text{-}d}$ is the peak power supply (Battery) discharge power, and η_m is the motor efficiency.

Hybrid propelling mode: If demanded power by driver for propelling is higher than engine can produce, which is indicated with point A in Figure 27, electric motors support

ICE. In this case power demand for ICE, which is defined as P_e, is selected according to ICE's optimum operating line (point a), and electric motors are responsible to provide remaining power demand. As a result, the motor power and PPS discharge power will be as follow.

$$P_m = P_L - P_e \tag{49}$$

$$P_{pps\text{-}d} = \frac{P_m}{\eta_m} \tag{50}$$

PPS Charge Mode: If demanded power by driver for propelling is lower than engine can produce while operating on its optimum operation line (point b), and SOC level is below predefined maximum and above predefined minimum value, then P_e, is selected according to ICE's optimum operating line (point b) and excessive power is used to charge battery. However, if SOC level is lower than predefined minimum value, ICE operates its maximum to charge battery as soon as possible. As a result, the input power to electric motor and PPS charge power according to SOC level will be as follow.

$$if\ SOC_{min} < SOC < SOC_{max}, \begin{cases} P_m = P_L - P_e \\ P_{pps\text{-}d} = \dfrac{P_m}{\eta_m} \end{cases} \tag{51}$$

$$if\ SOC < SOC_{min}, \begin{cases} P_m = P_L - P_{e\_max} \\ P_{pps\text{-}d} = \dfrac{P_m}{\eta_m} \end{cases} \tag{52}$$

Engine Alone Mode: If demanded power by driver for propelling is lower than engine can produce while operating on its optimum operation line (point b), and SOC level is reached predefined maximum value, then electric motors shut down and only ICE produce power as much as it is demanded (Point B in Figure 27). In this case ICE does not operate on its optimum operation line therefore some deficiency occurs. The engine power, electric power and battery power will be shown as follow.

$$P_e = P_L \tag{53}$$

$$P_m = 0 \tag{54}$$

$$P_{pps} = 0 \tag{55}$$

Regenerative Alone Brake Mode: If demanded braking power is less than the maximum braking regenerative power (Point C in Figure 27), then electric motors could be used as a generator to produce braking power and charge battery at the same time. As a result,

the electric power output which is produced by electric motors and charging power for battery will be expressed as follow.

$$P_{mb} = P_L \eta_m \tag{56}$$

$$P_{pps\text{-}c} = P_{mb} \tag{57}$$

Hybrid Braking Mode: If demanded braking power is greater than the maximum braking regenerative power (Point D in Figure 27), electric motors would not be sufficient and mechanical brake became necessary. In this case electric motor should be used at its maximum capacity and mechanical brake supply remaining brake power demand. As a result, the motor output power, PPS charging power, and mechanical braking power will be expressed as follow

$$P_{mb} = P_{mb,max} \eta m \tag{58}$$

$$P_{pps\text{-}c} = P_{mb} \tag{59}$$

$$P_{mf} = P_L - P_{mb} \tag{60}$$

The flowchart of the Maximum SoC Control Strategy is illustrated in Figure 28.

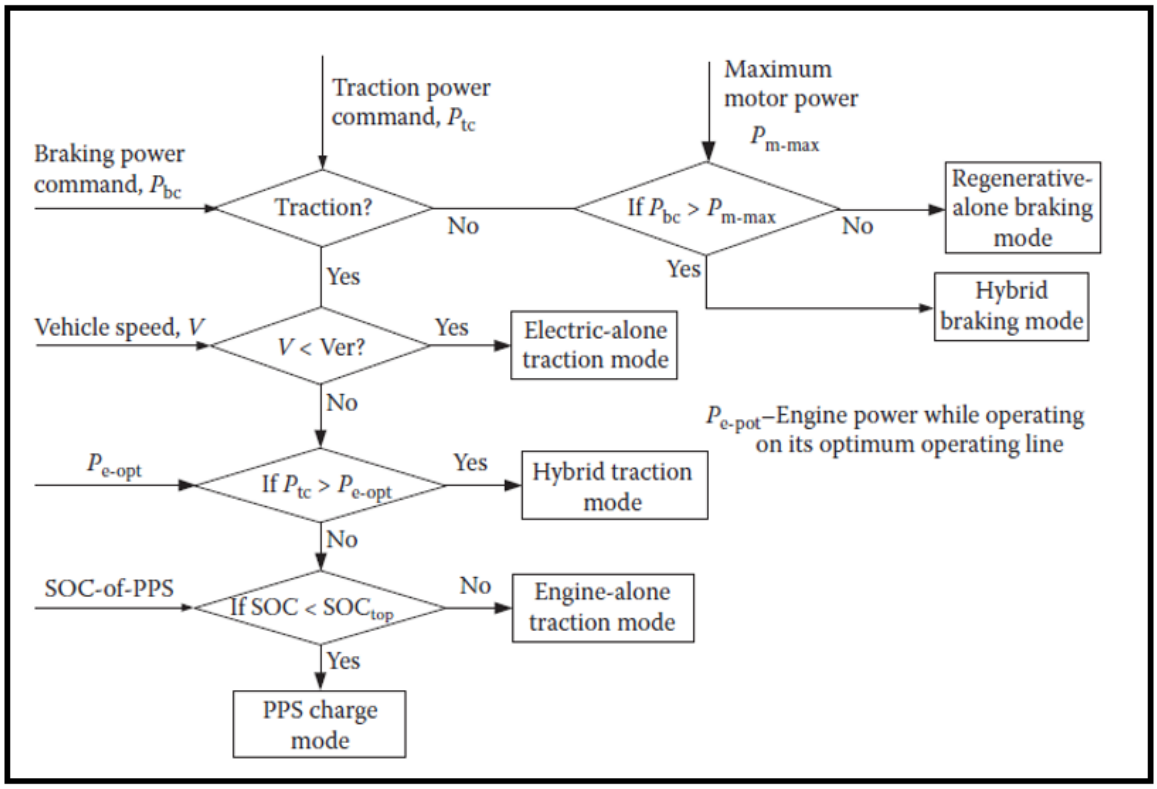

Figure 28: Flow Chart of Max SoC Control Strategy [33]

3.4.3. Direct Yaw Moment Control

In order to improve vehicle handling, direct yaw moment control is used to force the vehicle to follow reference vehicle behavior. In this method, the corrective yaw moment is generated by controlling transferred torque to the individual wheel. The generalized structure of the yaw controller system is described in Figure 29: Structure of Yaw Controller

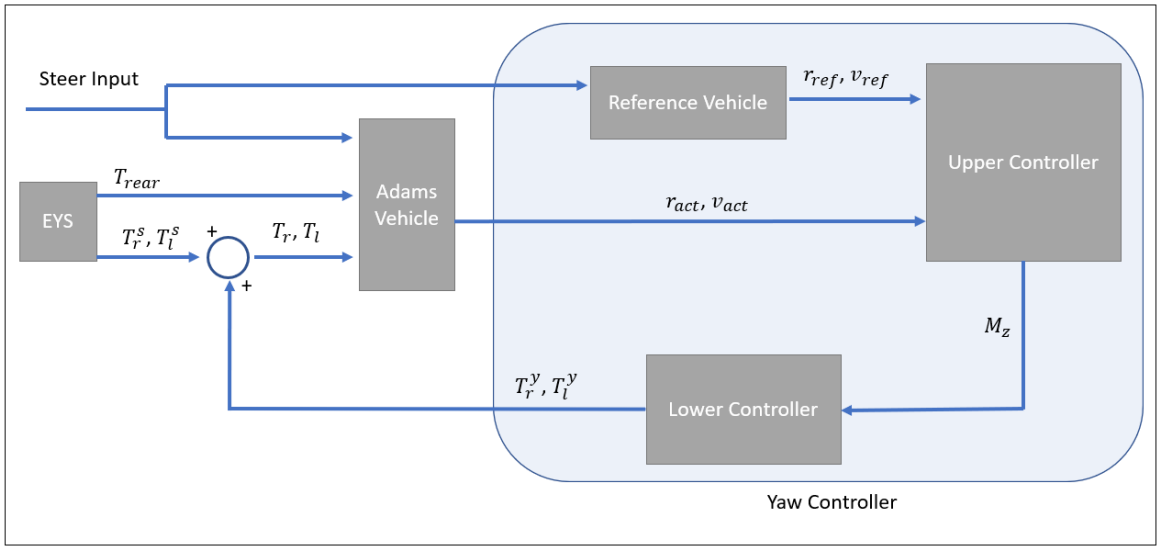

Figure 29: Structure of Yaw Controller

As shown above, the yaw controller consists of the upper controller, lower controller, and reference vehicle. The aim of the reference vehicle is to generate reference states for the upper controller, then the upper controller calculates the required yaw moment M_z to maintain vehicle yaw rate and lateral velocity which are specified by reference vehicle and the lower controller manages torque distribution among front wheels to produce corrective yaw moment.

In this chapter details of upper controller, reference vehicle and lower controller will be explained.

3.4.3.1. Reference Vehicle

The aim of the reference vehicle is generating the reference yaw rate (r_{ref})and lateral velocity (v_{ref}). Actual vehicle states (r_{act} & v_{act}) which are taken from Adams model, are subtracted from reference states then, the results are used for calculating control input M_z as shown in Figure 29. Therefore, reference vehicle needs to be ideal and produce proper states for better handling behavior as explained in section 2.2. Bicycle model is chosen to model reference vehicle with the following form

$$\dot{X} = A_{ref}X + E_{ref}\delta \tag{61}$$

Where

$$X_{ref} = \begin{Bmatrix} v_{ref} \\ r_{ref} \end{Bmatrix}, \qquad A_{ref} = \begin{bmatrix} -\frac{c_{f_{ref}} + c_r}{mu} & \frac{bc_r - ac_{f_{ref}}}{mu} - u \\ \frac{bc_r - ac_{f_{ref}}}{Iu} & -\frac{b^2c_r + a^2c_{f_{ref}}}{Iu} \end{bmatrix}, \qquad E = \begin{bmatrix} \frac{c_{f_{ref}}}{m} \\ \frac{ac_{f_{ref}}}{I} \end{bmatrix}$$

As seen above, the control input for the reference vehicle is steering input, and except for front cornering stiffness, all system variables are kept the same as the actual system. With this approach, it is intended to achieve similar behavior for reference vehicle with the actual vehicle but provide proper states from stable reference vehicle. As it is discussed in **Section 2.2** slightly positive k_{us} guarantee unconditionally stable system. After deciding proper k_{us} value, unknown cornering stiffness of reference vehicle is obtained with the following expression

$$c_{f_{ref}} = \frac{mbc_r}{k_{us}(a+b) + ma} \tag{62}$$

3.4.3.2. Upper Controller

The amount of the corrective yaw moment M_z is calculated by the upper controller based on the error between actual and desired vehicle yaw and lateral velocity states. To design

upper controller, the bicycle model with corrective yaw moment which is shown in Figure 30 is used.

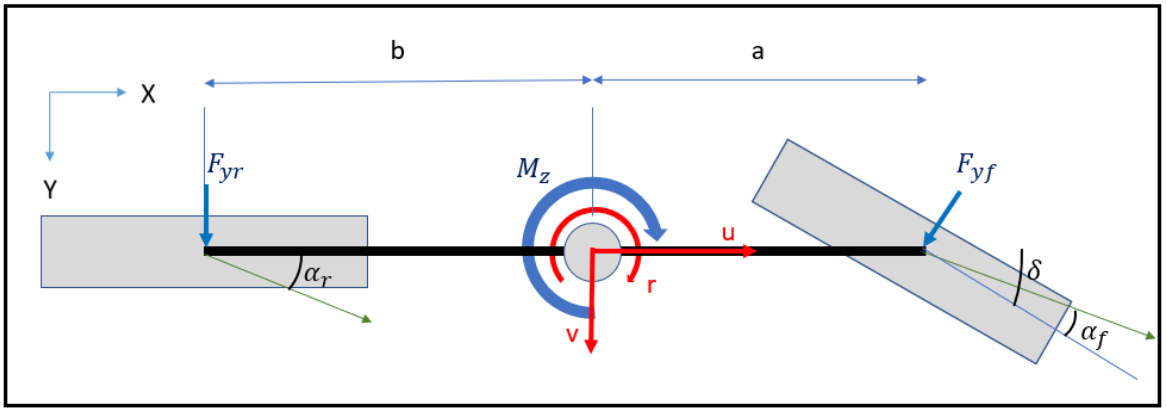

Figure 30: Linear Bicycle Model with M_z

By adding M_z into (25) we get following equations of motion.

$$m(\dot{v} + ur) = -(c_f + c_r)\frac{v}{u} + (bc_r - ac_f)\frac{r}{u} + c_f\delta \tag{63}$$

$$I\dot{r} = (bc_r - ac_f)\frac{v}{u} + (b^2c_r - a^2c_f)\frac{r}{u} + M_z + ac_f\delta \tag{64}$$

The above equations can be put into the general state space representation as follow

$$\dot{X} = AX + BM_z + E\delta \tag{65}$$

Where

$$X = \begin{Bmatrix} v \\ r \end{Bmatrix}, \quad A = \begin{bmatrix} -\frac{c_f + c_r}{mu} & \frac{bc_r - ac_f}{mu} - u \\ \frac{bc_r - ac_f}{Iu} & -\frac{b^2c_r + a^2c_f}{Iu} \end{bmatrix}, \quad B = \begin{bmatrix} 0 \\ \frac{1}{I} \end{bmatrix}, \quad E = \begin{bmatrix} \frac{c_f}{m} \\ \frac{ac_f}{I} \end{bmatrix}$$

Lateral velocity v and yaw rate r are state variables. On the other hand, steer input δ is the external disturbance of the system. Corrective yaw moment M_z is the control input.

The aim of the yaw controller is to manipulate states variables r and v for improving vehicle handling by using control input M_z. Hovewer control input M_z has limit in magnitude due to actutor size or some physical constraints such as friction circle. Therefore, considering limitation leads us to design linear quadratic regulator for this problem.

The control law for input M_z consist of two state variable feedback terms yaw rate and lateral velocity.

$$M_z = -(K_r r + K_v v) \tag{66}$$

For the linear system (65), a quadratic cost function defined as

$$J = \int_0^\infty \left(X^T Q X + {M_z}^T R M_z\right) dt \tag{67}$$

Where Q is positive semi definite and R is positive definite weighting functions. On the other hand, the control law is in the following form.

$$M_z = -KX \tag{68}$$

Where

$$K = R^{-1} B^T S$$

Where S symmetric 2 by 2 matrix and it is the solution of Algebraic Ricatti Equation.

$$A^T S + SA - SBR^{-1}B^T S + Q = 0 \tag{69}$$

There are 4 solution of equation (70), therefore one can find 4 different set of S matrix and feedback gain. However only one solution could result with stable system. After

obtaining feedback gain candidates (U), by solving following eigenvalue problem correct set of feedback gain could be gained.

$$|A - BU| = 0 \tag{71}$$

Set of feedback gain pair which results with negative eigenvalue, are the optimal values for yaw controller.

3.4.3.3. Lower Controller

The lower controller is responsible for creating corrective yaw moment which is calculated by upper controller. It takes M_z as an input and produce torque demand for right and left wheels.

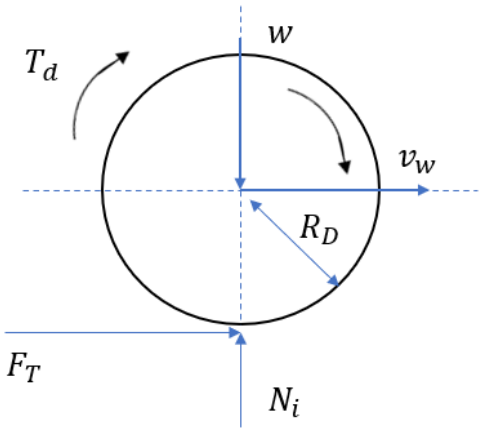

Figure 31: Rotational Dynamics of Wheel

Equation of motion for a wheel according to free body diagram which is illustrated in Figure 31, with no slip assumption can be written as follow.

$$T - R_D F_T = J_w \dot{w} \tag{72}$$

In the above expression, T is the applied torque on wheel, R_D is dynamic radius of wheel, F_T is traction force on contact point, J_w is wheel's moment of inertia about its axis of

rotation and *w* is angular velocity of wheel. With assuming steady state condition, traction force became proportional to applied torque.

$$T_l = RF_l \quad \& \quad T_r = RF_r \tag{73}$$

If applied torques on right and left wheels differ, traction forces also differ at right and left wheel contact points which is described in Figure 32.

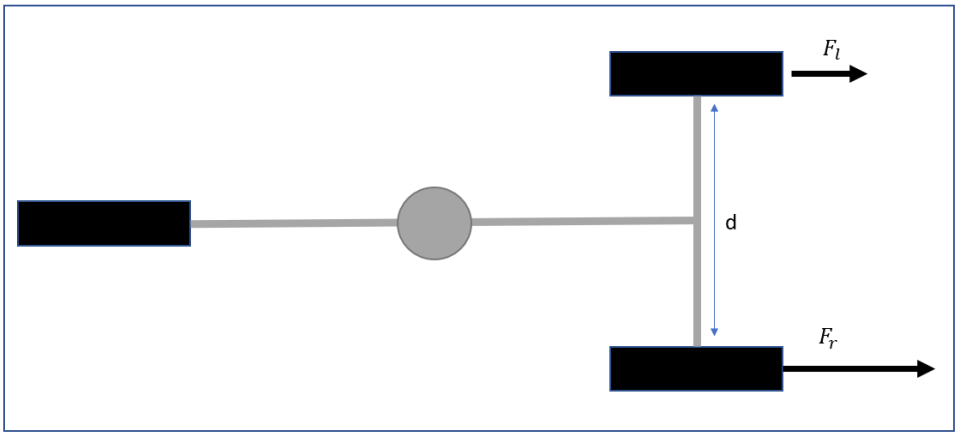

Figure 32: Yaw Moment Generation

Note that torque on wheel hub *T* is summation of required torque for longitudinal speed demand T^s and required torque for corrective yaw moment T^y. T^s is equal for each wheel on the other hand T_r^y and T_l^y are same in magnitude but opposite direction in order to differ torque and generate yaw moment eventually.

$$T_l^y = -T_r^y = \frac{M_z}{2d} \tag{74}$$

4. SYSTEM EVALUATION

In this study, the yaw stability controller and energy management system were designed and modeled for a three-wheeled hybrid vehicle. It is claimed, three-wheeled vehicles are more efficient thanks to the energy management system, more stable thanks to the yaw stability system and finally, both torque management systems are compatible, and they can be used together. In this chapter, all three claims will be evaluated.

4.1. Evaluation of Energy Management System

The aim of the EMS is to decrease fuel consumption. Therefore, it is expected to obtain better fuel efficiency from the hybrid vehicle with respect to the similar vehicle which runs only the internal combustion engine. In this chapter, the performance comparison will be illustrated. ICE model of the hybrid vehicle is used again for a conventional vehicle.

4.1.1. Test Maneuver

The driving cycle is derived from the US FTP-72 which is illustrated in Figure 33. US FTP-72 cycle is also called Urban Dynamometer Driving Schedule (UDDS). Complete stops cause some stability problems in Adams model, hence minimum velocity is slightly higher than zero in our simulation. Because of frequent stops, UDDS simulates urban driving and used for light duty vehicles [37]. Average speed of the cycle is $31.51\ km/h$, maximum speed is $91.25\ km/h$, maximum acceleration is $1.48\ m/s^2$ and maximum deceleration is $-1.48\ m/s^2$.

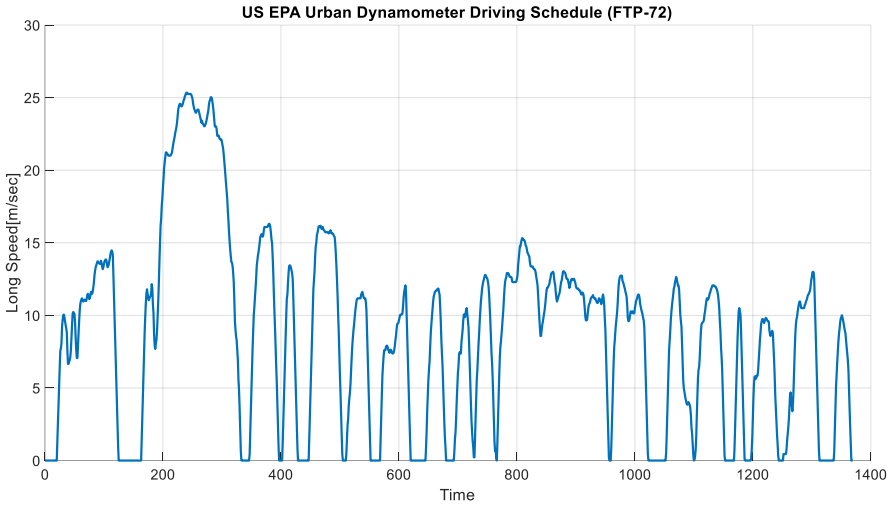

Figure 33: The US FTP-72

4.1.2. Test Results

Before comparing fuel efficiency performance, it is required to show that vehicle able to follow drive cycle. According to Figure 34 and Figure 35 it can be said that both vehicles can follow the desired drive cycle speed sufficiently.

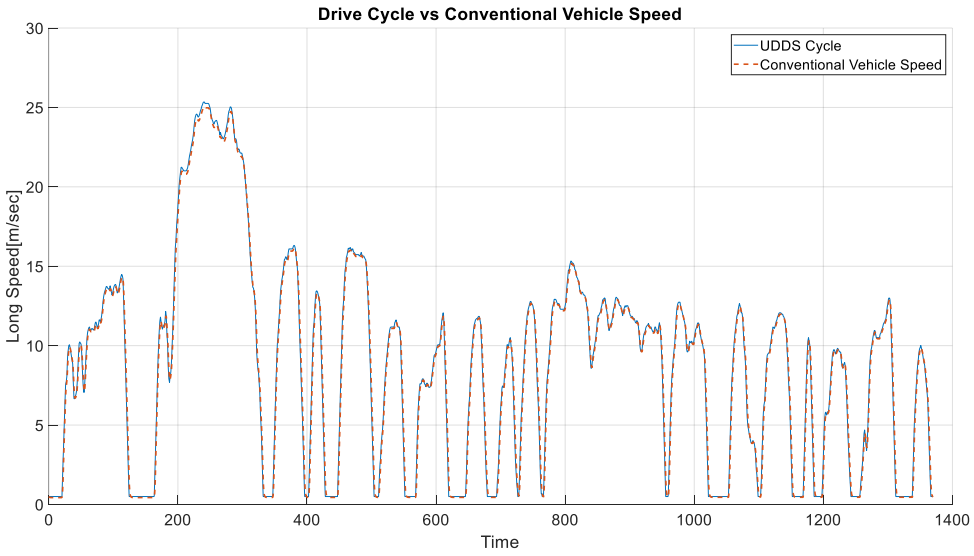

Figure 34: Conventional Vehicle Speed Performance

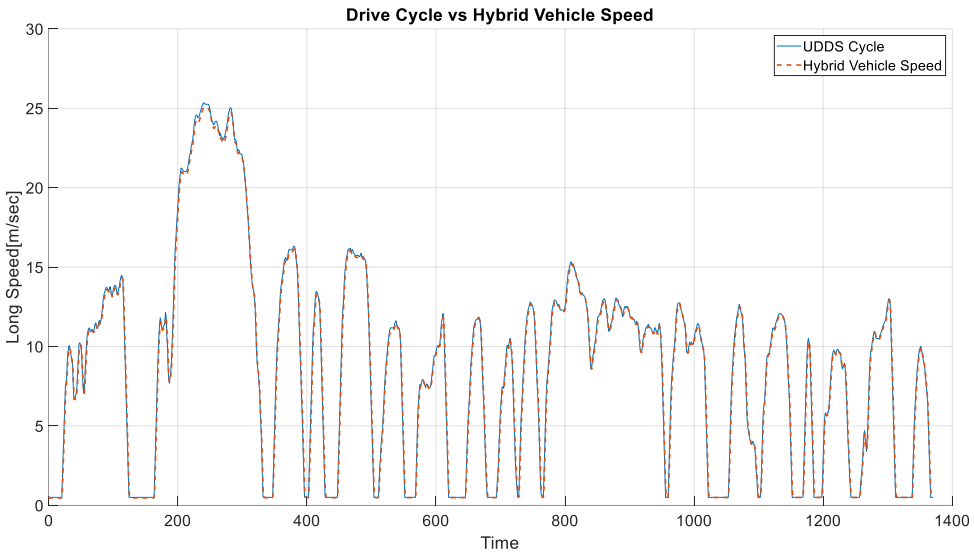

Figure 35: Hybrid Vehicle Speed Performance

As explained section 3.4.1 and 3.4.2, to follow desired speed, speed controller calculates required torque then EMS decide the portion of each power source. EMS output is illustrated in Figure 36. It shows, requested torque from electric motors and ICE in time. It can be seen that electric motors are assigned to start motion alone and ICE does not contribute until vehicle speed reach 11.1 m/sec. For higher speed, ICE running and produce torque on its optimum operating line while torque output from electric motors is varying to supply peak power to drive train. During motor-alone propelling mode, ICE does not transmit torque, but it runs at the idle speed which is 800 rpm (Figure 37). Also, negative spikes occurred during the simulation for electric motors contrast to ICE because of regenerative breaking.

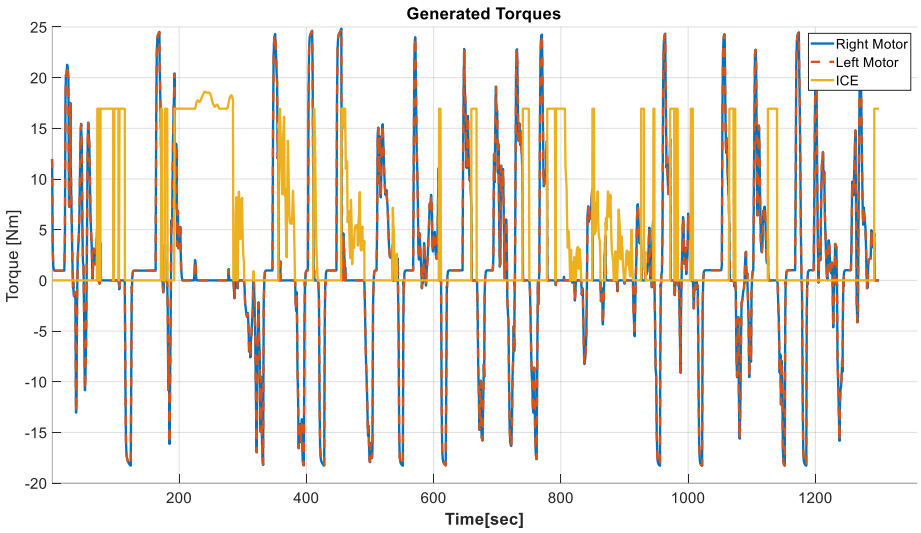

Figure 36: Generated Torque Distribution among Power Sources

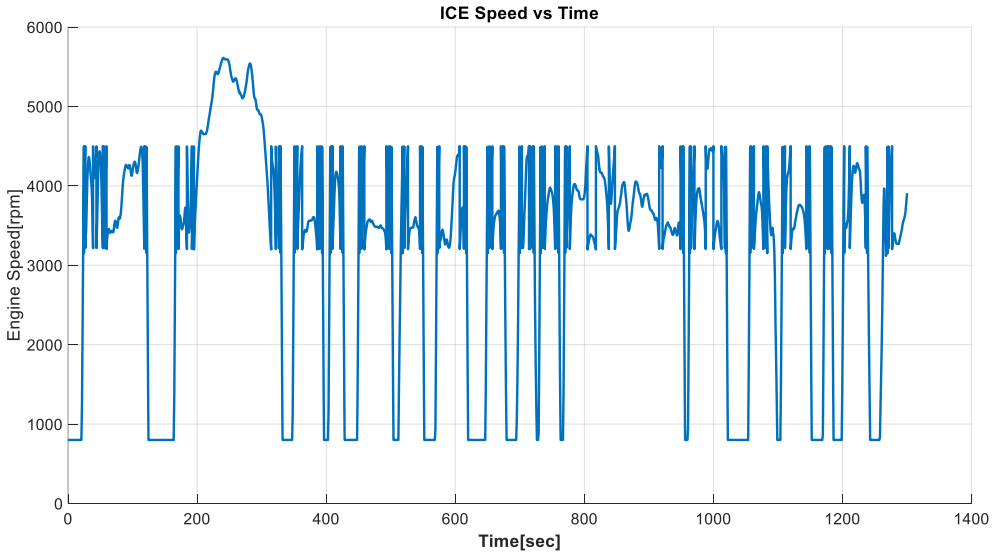

Figure 37: ICE Speed vs Time

The effect of torque distribution could be seen in longitudinal tire forces as well. All traction effort must be supplied from rear axle for the conventional vehicle (Figure 38). Therefore, front wheel tire forces of conventional vehicle never be positive (Figure 39,Figure 40).

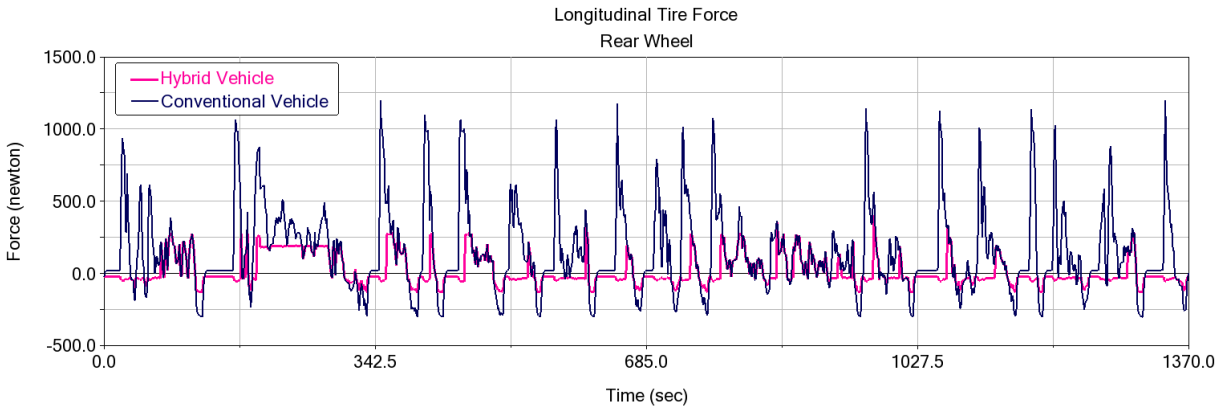

Figure 38: Rear Wheel Longitudinal Tire Force

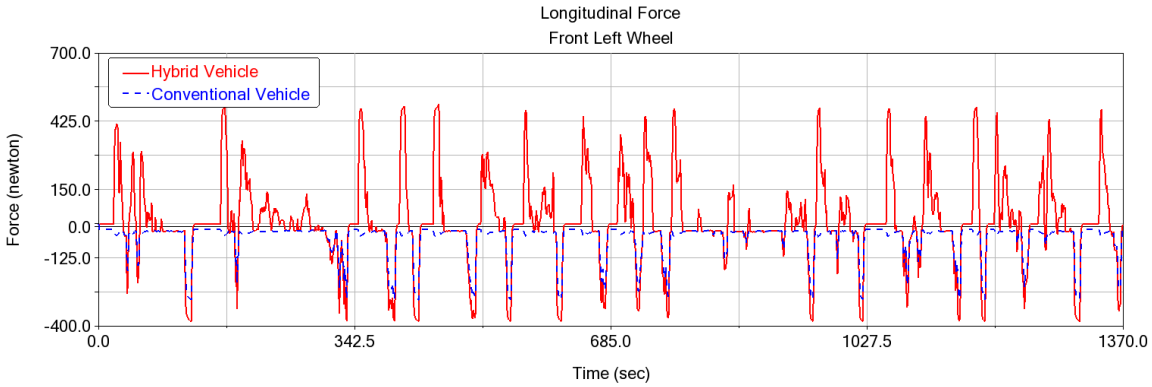

Figure 39: Left Wheel Longitudinal Tire Force

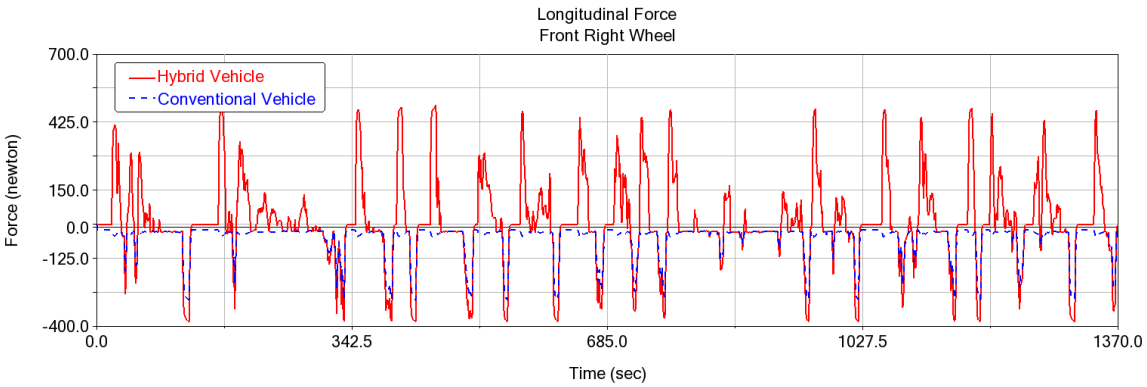

Figure 40: Right Wheel Longitudinal Tire Force

Examining the state of charge level and EMS modes with respect to time which is depicted in Figure 41, gives better insight into the behavior of the EMS. During the hybrid mode and the motor alone mode SoC level is decreasing. However, PPS Charge and

Regenerative Braking mode cause increasing in SoC level. Note that SoC level is start from 75 and its final value is 77.

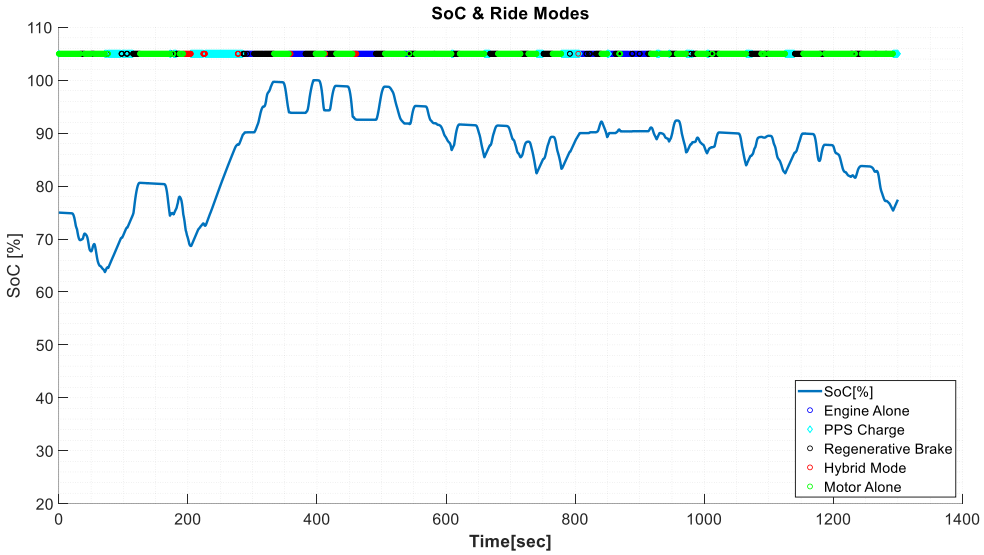

Figure 41: SoC & Ride Modes

Finally, Figure 42 shows the fuel consumption of the hybrid vehicle and conventional vehicle over the same drive cycles. According to the results, the conventional vehicle consumed 0.36-liter fuel, on the other hand, fuel consumption for the hybrid vehicle is obtained as 0.25 liter. Recovering brake energy and running ICE on its efficient operating line results in a 30% drop in fuel consumption.

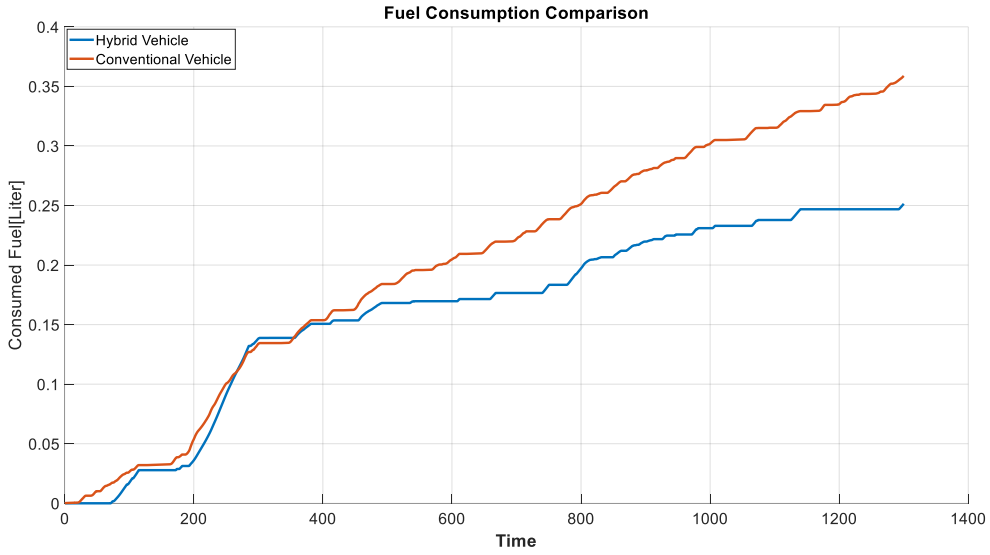

Figure 42: Fuel Consumption Comparison

4.1.3. Summary

It is shown that both conventional vehicle and hybrid vehicle analyses are performed successfully. During the simulation, EMS forced ICE to run at its efficient operation line. At the same time, EMS managed electric motors to supply peak power and follow the drive cycle sufficiently. As a result, %30 fuel efficiency is obtained compared to conventional vehicle thank to the energy management system.

4.2. Evaluation of Yaw Controller

The aim of the yaw controller is to improve vehicle handling. Therefore, the vehicle with the yaw controller is supposed to respond to driver inputs with better handling quality and provide stability during cornering. In this chapter yaw controller performance will be investigated by performing ramp steer input and double lane change analyses. During analysis, EMS is going to be inactive, but torque vectoring will be done by electric motors.

4.2.1. Test Maneuver

Test maneuvers, ramp input at a constant velocity and Iso Double Lane Change analyses are described as follow.

4.2.1.1. Ramp Steer Test Maneuver

During the simulation, vehicle velocity is kept constant at 72 km/h and a ramp signal is applied to the steering angle. The vehicle moves on a flat and dry road with peak friction of coefficient equals 1. The steering angle ramp is chosen as 1.0 degree/second. With this test maneuver, vehicle handling characteristics and the effect of the yaw controller on it will be investigated.

4.2.1.2. ISO Double Lane Change Test Maneuver

ISO Double Lane Change is a close loop test maneuver that is used to investigate vehicle lateral dynamics and considered suitable for evaluating electronic stability control system according to research institutions. In this test maneuver, the vehicle must follow the path, which is defined by ISO 3888 standard, under a professional driver's control. MSC Adams Car provides the trajectory (Figure 43) and driver model for steering. During simulation, the lateral distance between the reference marker, which is positioned near to center of gravity, and trajectory is captured, and steer input demand is calculated automatically by MSC Adams Car. Entry speed is chosen as 72 km/h.

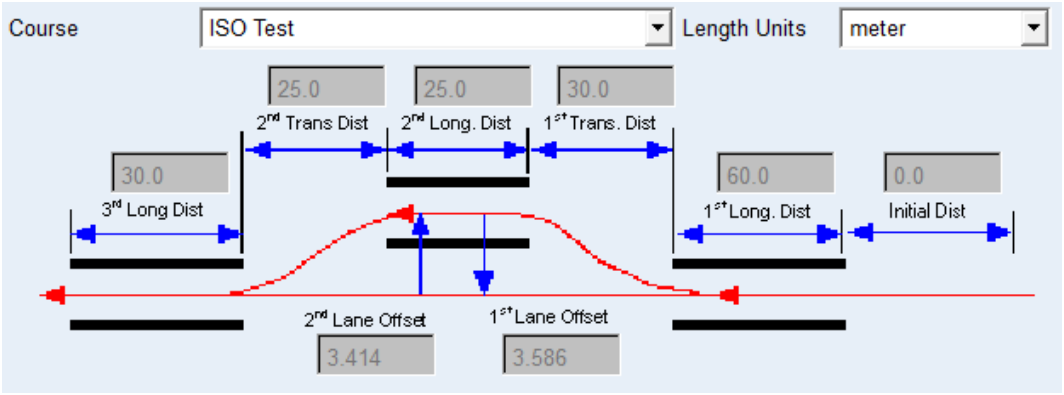

Figure 43: ISO Double Lane Change Trajectory

4.2.2. Test Results

4.2.2.1. Test results of Ramp Steer Test Maneuver

Analysis results clearly show that the three-wheeled vehicle has oversteer characteristic and unable to remain stable. As illustrated in Figure 44 yaw response of vehicle without

torque vectoring, increase exponentially after 85 second and vehicle spins off. On the other hand, the yaw response of the vehicle with torque vectoring is linear with respect to linear steer input and the vehicle remains stable throughout the simulation.

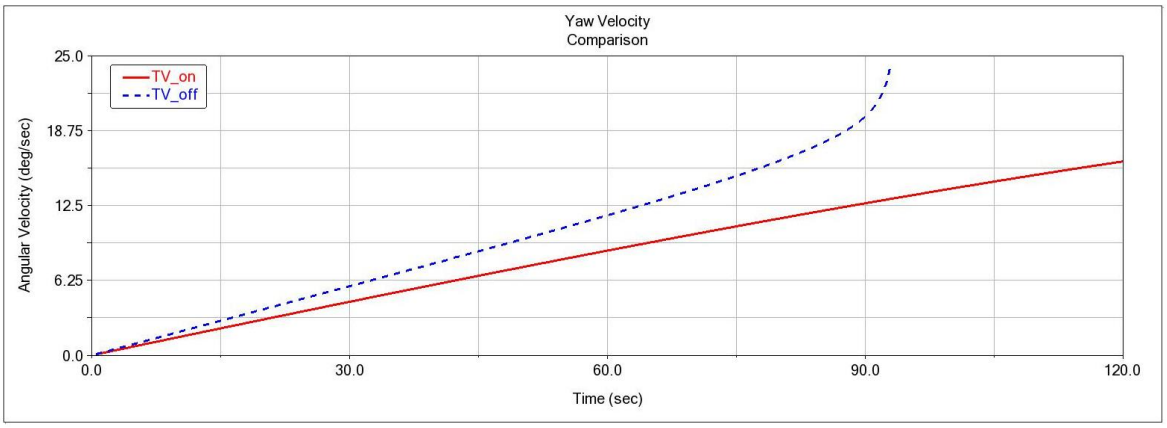

Figure 44: Yaw Response Comparison

When torque vectoring is active, right and left electric motors produce and transmit torque to wheels in opposite direction to generate yaw moment. At that time longitudinal velocity is kept constant by ICE. Torque distribution is depicted in Figure 45.

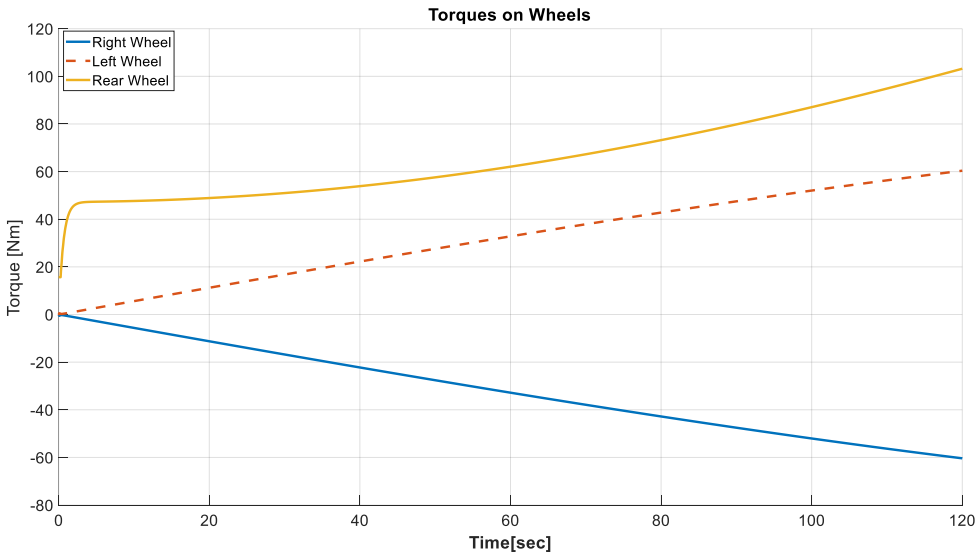

Figure 45: Generated Torques among Power Sources

4.2.2.1. Test results of ISO Double Lane Change Test Maneuver

Simulation results which are longitudinal velocity, yaw velocity, lateral velocity, and side slip angle comparison for controlled and uncontrolled cases are shown in Figure 47 through Figure 49. Also, absolute values of minimum longitudinal velocities, maximum yaw ,and lateral velocities ,and maximum side slip angle are indicated in Table 7 .

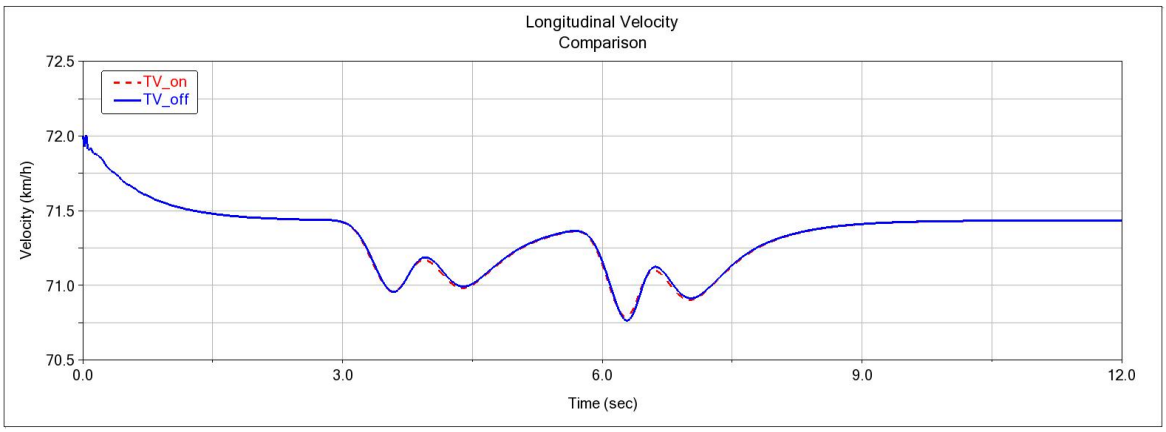

Figure 46:Longitudinal Velocity Comparison

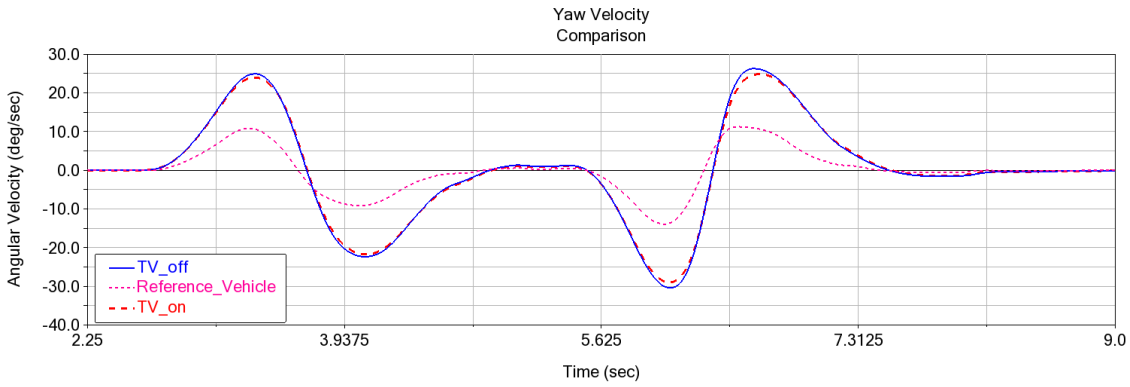

Figure 47: Yaw Velocity Comparison

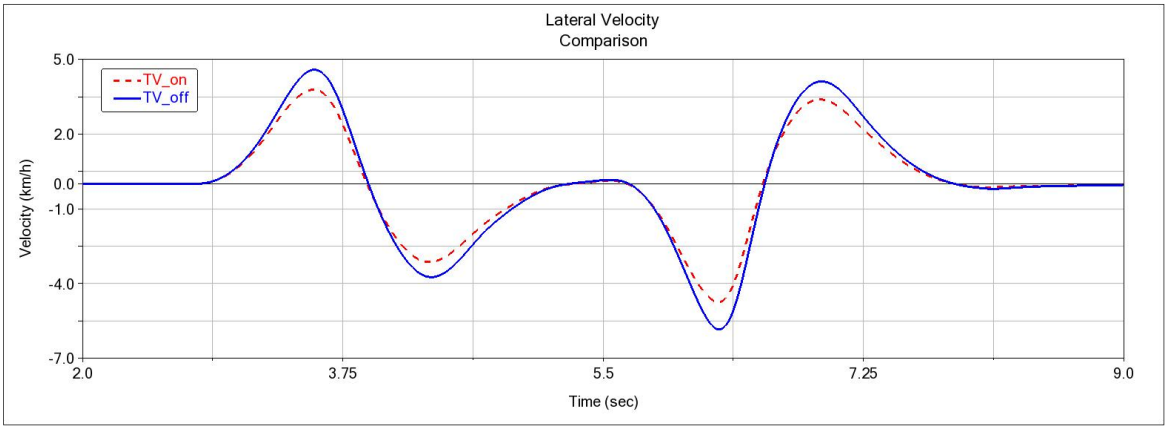

Figure 48:Lateral Velocity Comparison

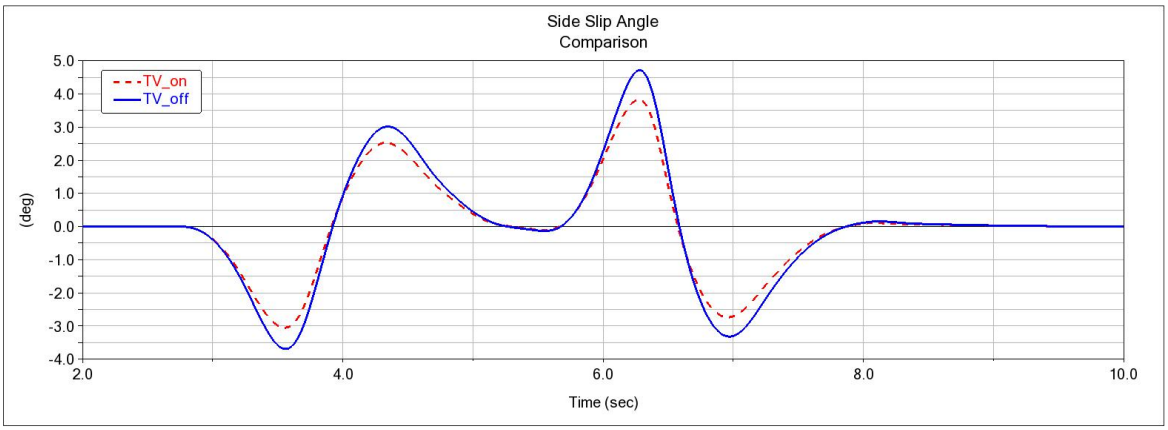

Figure 49: Side Slip Angle Comparison

Table 7: Double Lane Change Analysis Results

	$u_{min}[km/h]$	$\|r\|_{max}[deg/sec]$	$\|v\|_{max}[km/h]$	$\|\beta\|_{max}$[ang]
TV On	70.8	28.2	4.7	3.8
TV Off	70.8	30.4	5.8	4.7
$\left(\left\|x_{on} - x_{off}\right\| / x_{off}\right)$	0%	7.2%	19.0%	19.1%

The torques from electric motors to generate yaw moment is depicted in Figure 50.

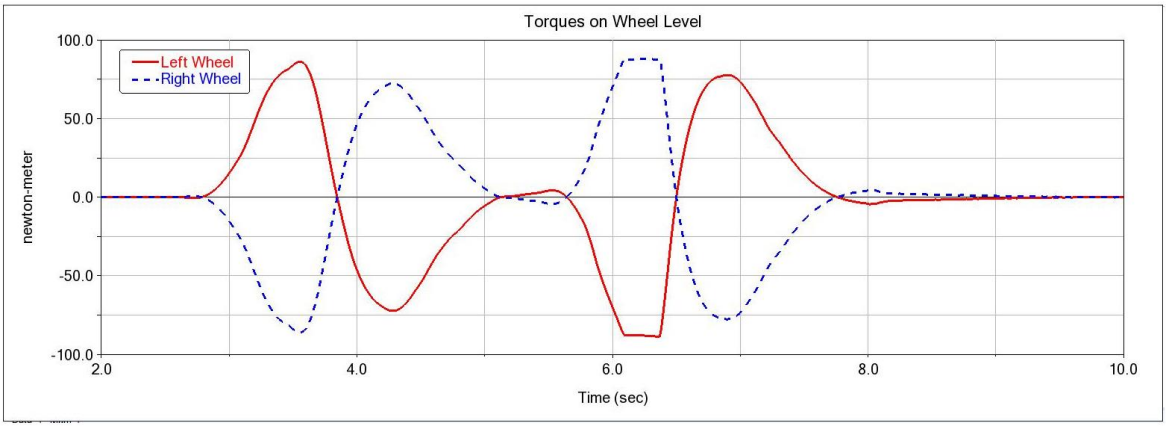

Figure 50: Torques on Wheel Level

Main observation from double lane change analysis is that yaw controller is capable of decreasing yaw velocity 7.2%, lateral velocity and slip angle 19% without causing speed loss during maneuver.

4.2.3. Summary

In the light of results of both steer ramp and double lane change analysis for the controlled and uncontrolled three-wheeled vehicle, it can be concluded that the yaw controller has a significant effect on vehicle handling characteristics. The yaw controller is able to improve handling quality, change oversteer tendency of the vehicle into understeer characteristic and keep the vehicle stable during harsh maneuver by managing torque distribution among front wheels.

4.3. Evaluation of Combined System

The purpose of this section is to examine the compatibility of EMS and DYC. The test maneuver to activate both systems must include steer input and acceleration demand. The necessity of acceleration is due to the nature of parallel hybrid drivetrain because the size of ICE in the parallel hybrid drivetrain is capable to maintain constant velocity cruise, thus only "PPS Charge Mode" and "Engine Alone Mode" can be monitored without acceleration. On the other hand, acceleration demand causes the change from “Engine Alone Mode” to “Hybrid Mode” or “Hybrid Mode” to “PPS Charge Mode” that results

in a change in lateral dynamics behavior of the vehicle and perhaps the conflict between EMS and DYC.

Top speed, acceleration, SoC level, and surface frictions can have different results. In each analysis, we will differentiate one variable and keep the others constant in order to reach a general opinion. Comparisons will be made for a conventional vehicle, hybrid vehicle, and hybrid vehicle with DYC.

4.3.1. Test Maneuver - 1

Test Maneuver - 1 is designed to investigate effect of EMY and combined system on lateral dynamics with the following parameters:

Table 8: Test Maneuver - 1 Parameters

Initial Longitudinal Speed $[m/s]$	10
Maximum Longitudinal Speed$[m/s\ ]$	20
Acceleration $[m/s^2\ ]$	0.5
Maximum Steer Input[degree]	25
Friction Coefficient	1
[Initial,Min,Max] SoC	75,60,90

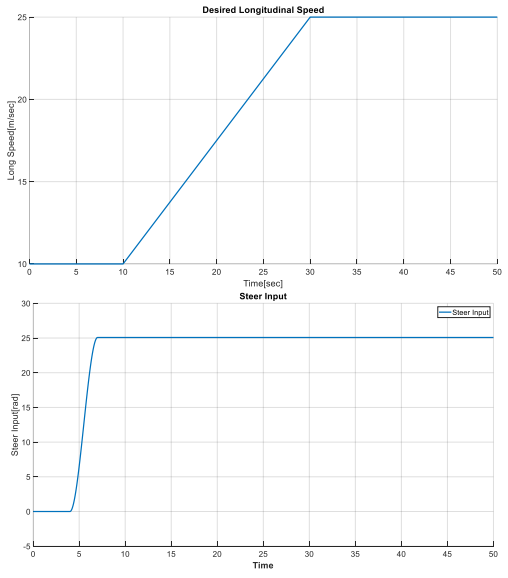

Note that parameters of Test Maneuver-1 do not contain any extreme case, therefore it can be called base model.

4.3.1.1. Results

According to Figure 51 the vehicle reached the same longitudinal velocity for three cases without spin. In addition, it can be seen from Figure 52, the support of the electric motors to the combustion engine remained limited. A similar observation could be made by looking at Figure 53, while ICE transmitted 10 kW of power, the total power transmitted by electric motors around 2 kW. As a result, there is not a significant difference in lateral dynamics between the hybrid vehicle and the conventional vehicle. On the other hand, enhancement for the case in which torque vectoring is activated is obvious.

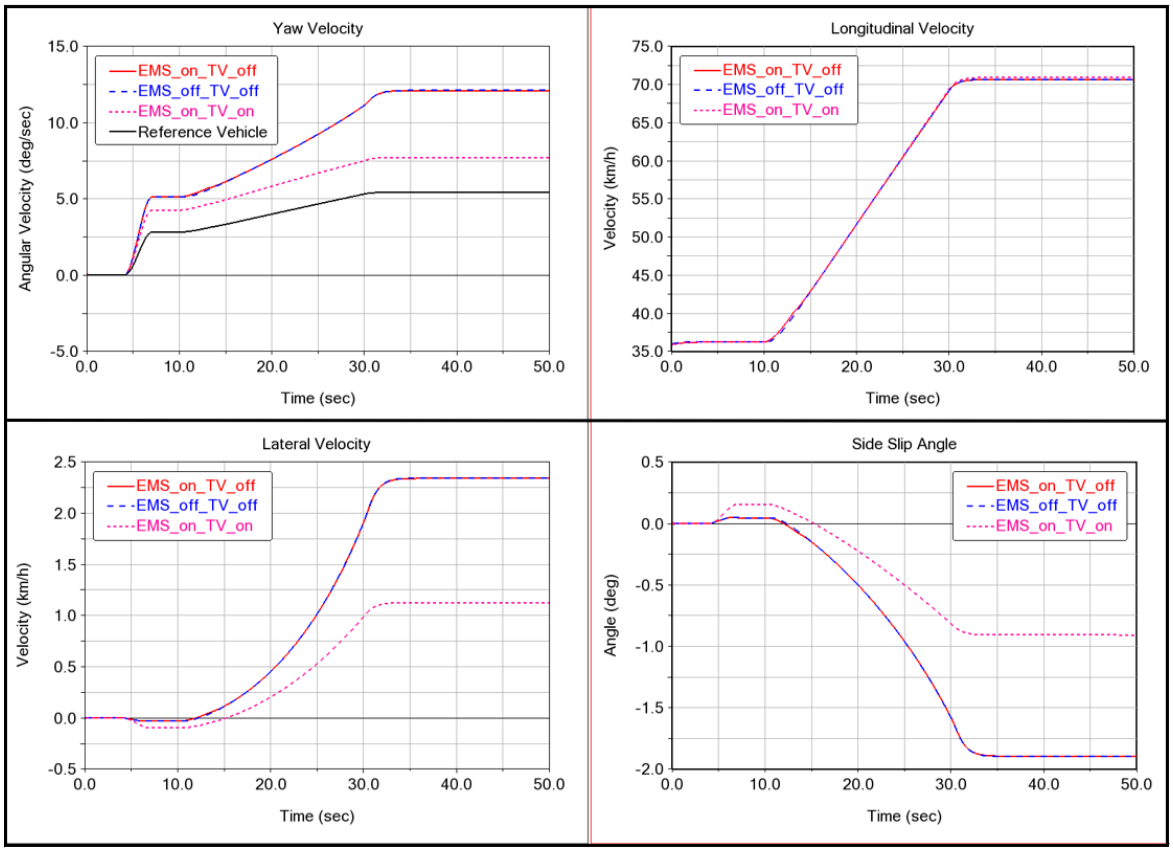

Figure 51:Vehicle Responses

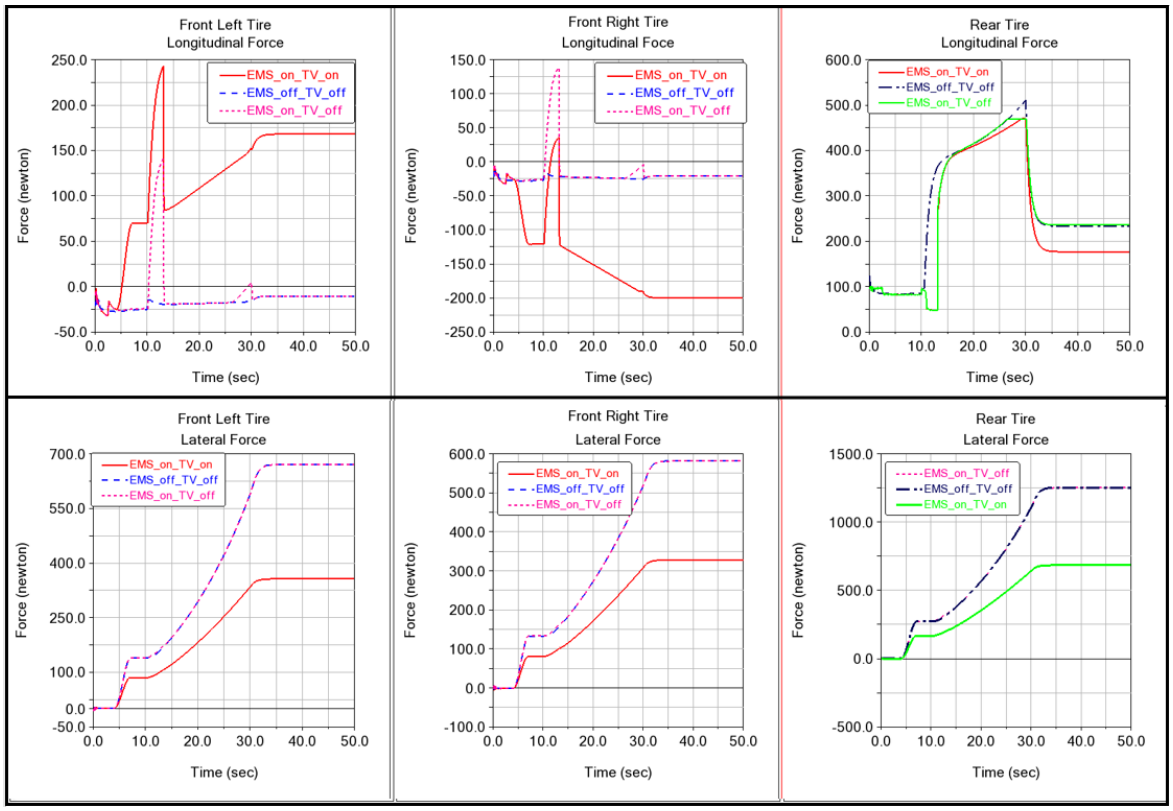

Figure 52: Tire Forces

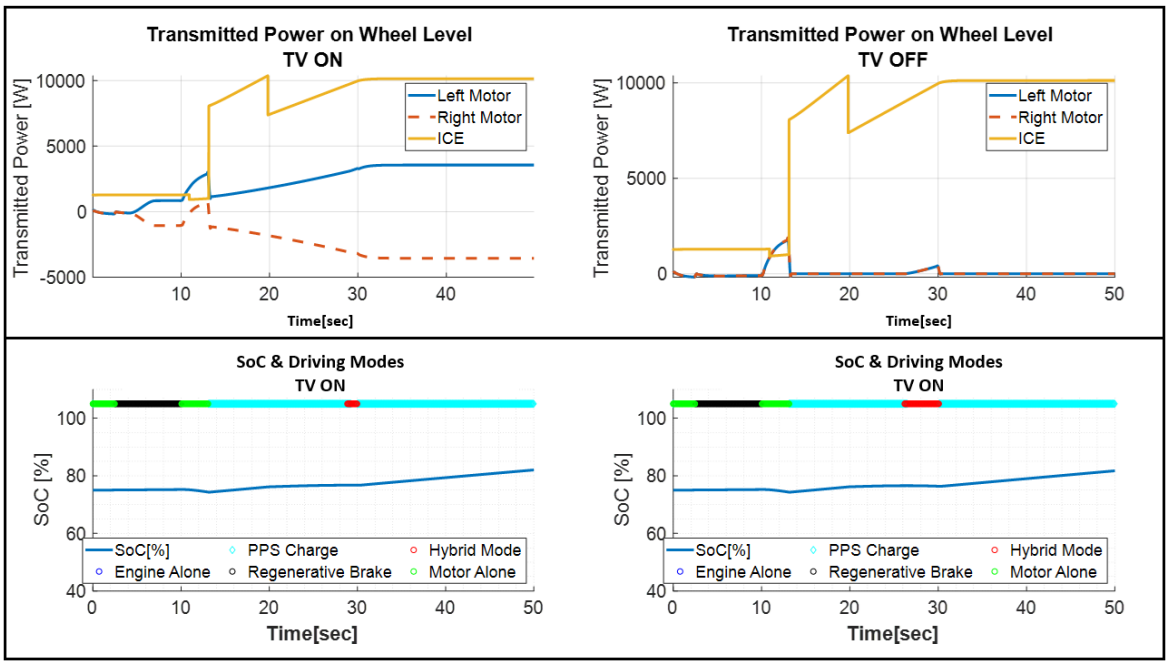

Figure 53: Transmitted Power & Battery Level

4.3.2. Test Maneuver – 2

Test Maneuver – 2 is designed to compare effect of acceleration with relative to base model. Parameters of Test Maneuver – 2 are given below. Not that acceleration is increased from 0.5 m/s^2 to 1 m/s^2 and other variables are kept same.

Table 9: Test Maneuver – 2 Parameters

Initial Longitudinal Speed [m/s]	10
Maximum Longitudinal Speed[m/s]	20
Acceleration [m/s^2]	1
Steer Input[degree]	25
Friction Coefficient	1
[Initial,Min,Max] SoC	75,60,90

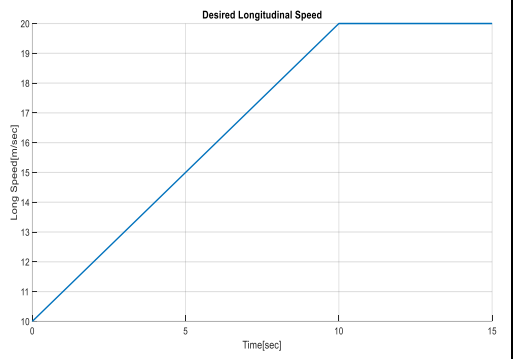

4.3.2.1. Results

With respect to Test Maneuver - 1, although the final speed remains the same, the time to reach the final speed is shorter in Test Maneuver – 2. An increase in acceleration is achieved by applying more traction force. Since the highest available power rating in the hybrid vehicle, the hybrid vehicle shows slightly better longitudinal performance between 7 and 11 seconds (Figure 54). When we look at the yaw response, we can think that around the 11th seconds the hybrid mode causes higher-than-expected yaw velocity. However, the reason behind that is the vehicle reached a higher speed at that time with hybrid mode. In other words, the conventional vehicle produced less yaw velocity, because it is slower than the hybrid vehicle. As shown in Figure 55, the wheel forces increased in the longitudinal direction, but could not reduce the lateral forces as force magnitude could not reach the friction limit. Therefore, the vehicle response results of Test Maneuver - 1 and Test Maneuver – 2 were obtained very similarly.

Another remarkable observation is depicted in Figure 56, in the case where the torque vectoring is active, ICE generates less power because the lateral force generated by the rear wheel is decreased with the corrective yaw moment.

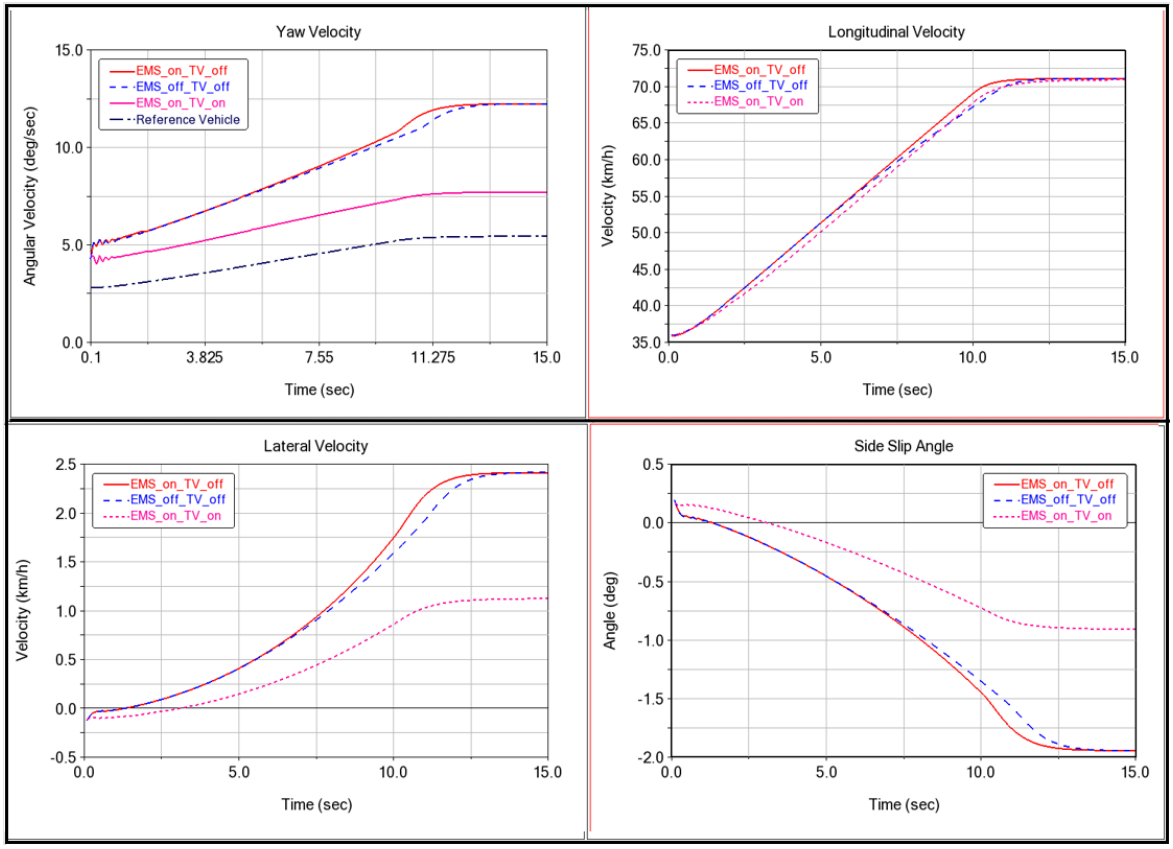

Figure 54: Vehicle Response

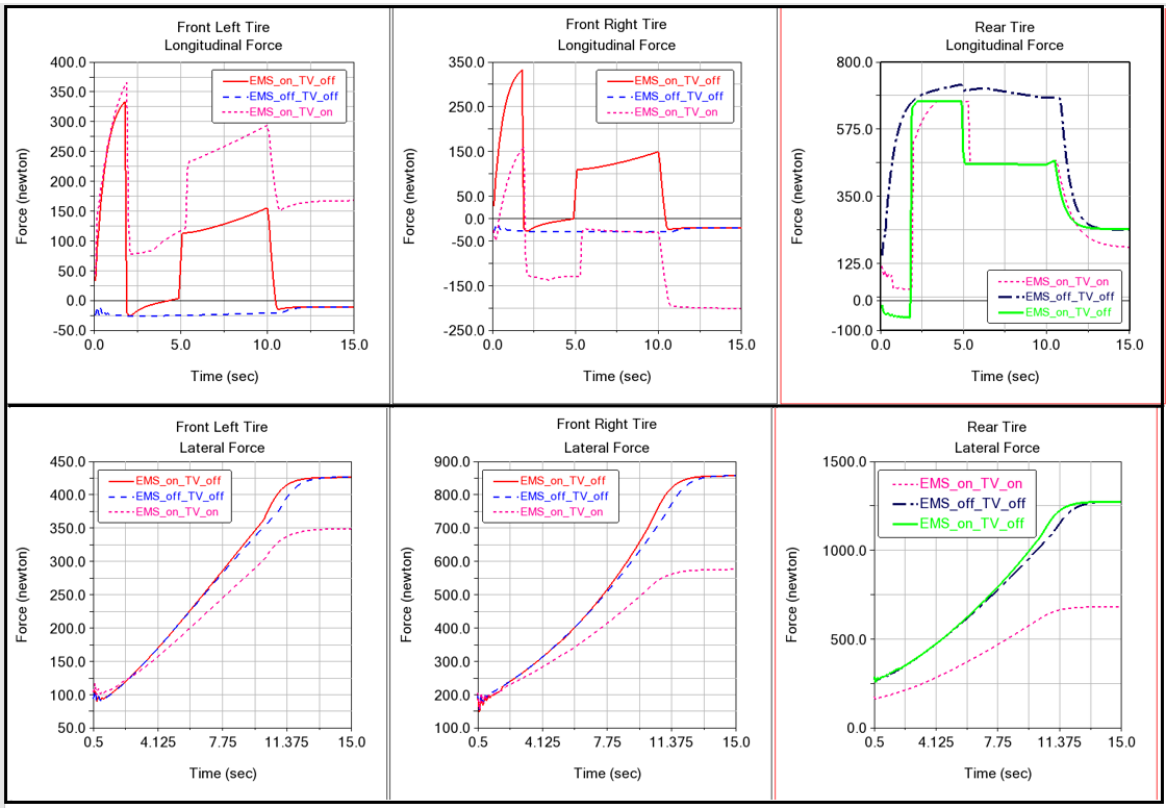

Figure 55: Tire Forces

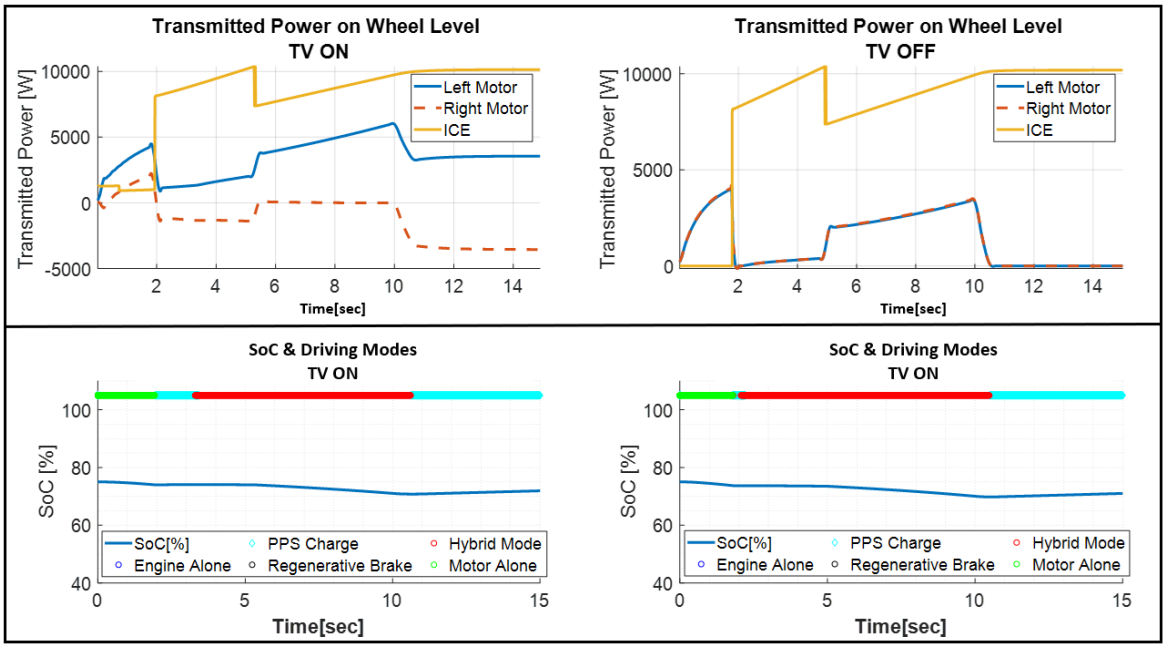

Figure 56: Transmitted Power & Battery Level

4.3.3. Test Maneuver – 3

In Test Maneuver – 3, top speed is increased to 25 m/s , other parameters are given below.

Table 10: Test Maneuver – 3 Parameters

Initial Longitudinal Speed [m/s]	10
Maximum Longitudinal Speed[m/s]	25
Acceleration [m/s^2]	0.75
Steer Input[degree]	25
Friction Coefficient	1
[Initial,Min,Max] SoC	75,60,90

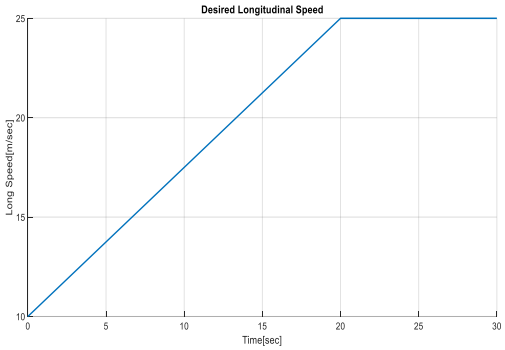

4.3.3.1. Test Result

It can be said that according to Figure 58, as the speed increased, the lateral force on the wheels due to the side slip angle increased. In the hybrid and conventional vehicle situations, the rear wheel reached the limit and the vehicle starts to spin when it could not generate more lateral force. As in previous cases, there is no significant difference between the hybrid vehicle and conventional vehicle, except that the hybrid vehicle has a slightly better longitudinal performance. In the case of a hybrid vehicle with torque vectoring, it was sufficient for the rear tire to generate less force due to the generated yaw moment and the vehicle remained stable.

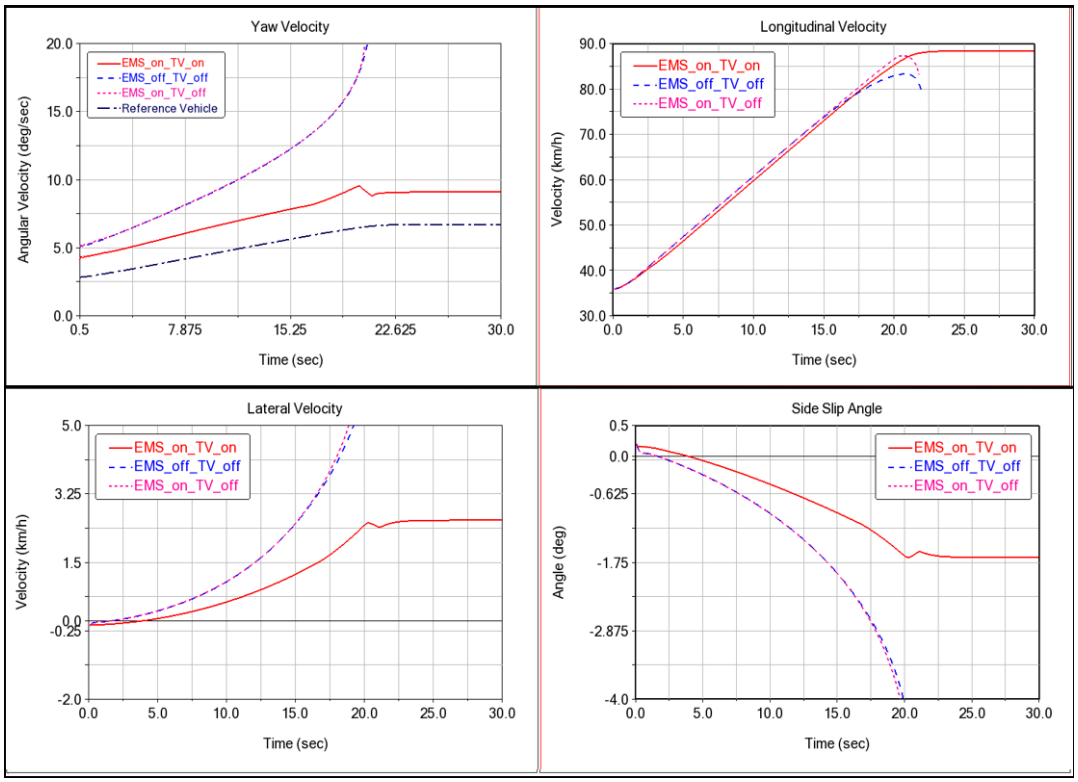

Figure 57: Vehicle Response

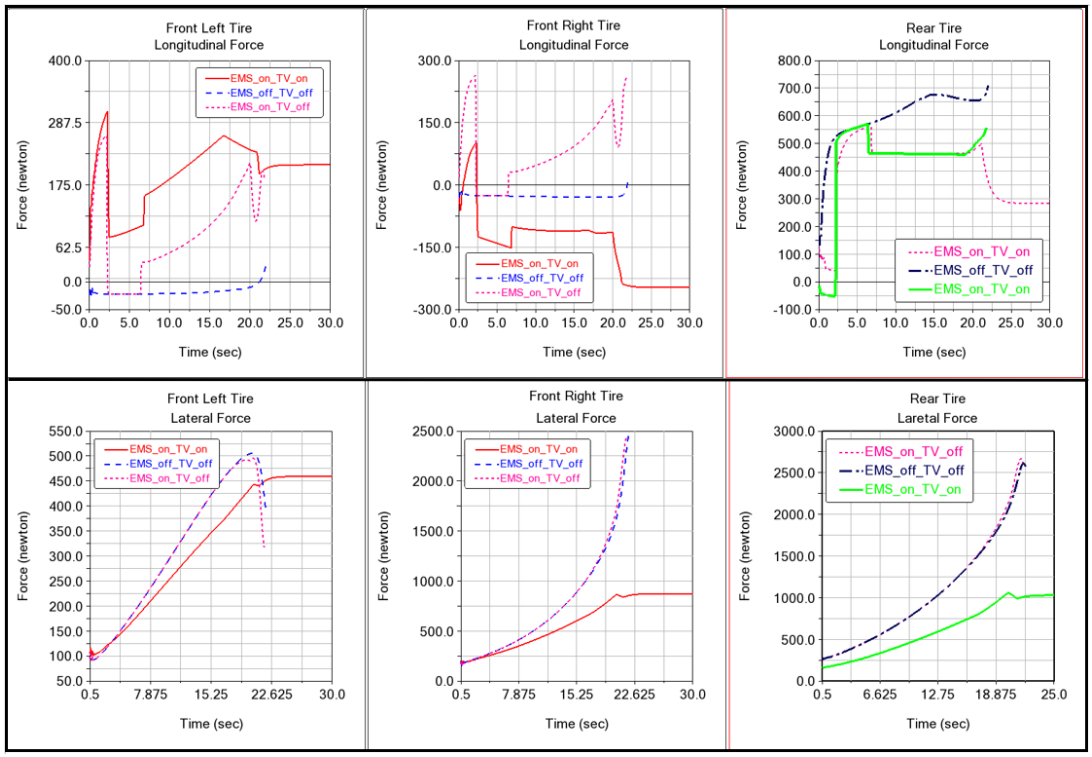

Figure 58: Tire Forces

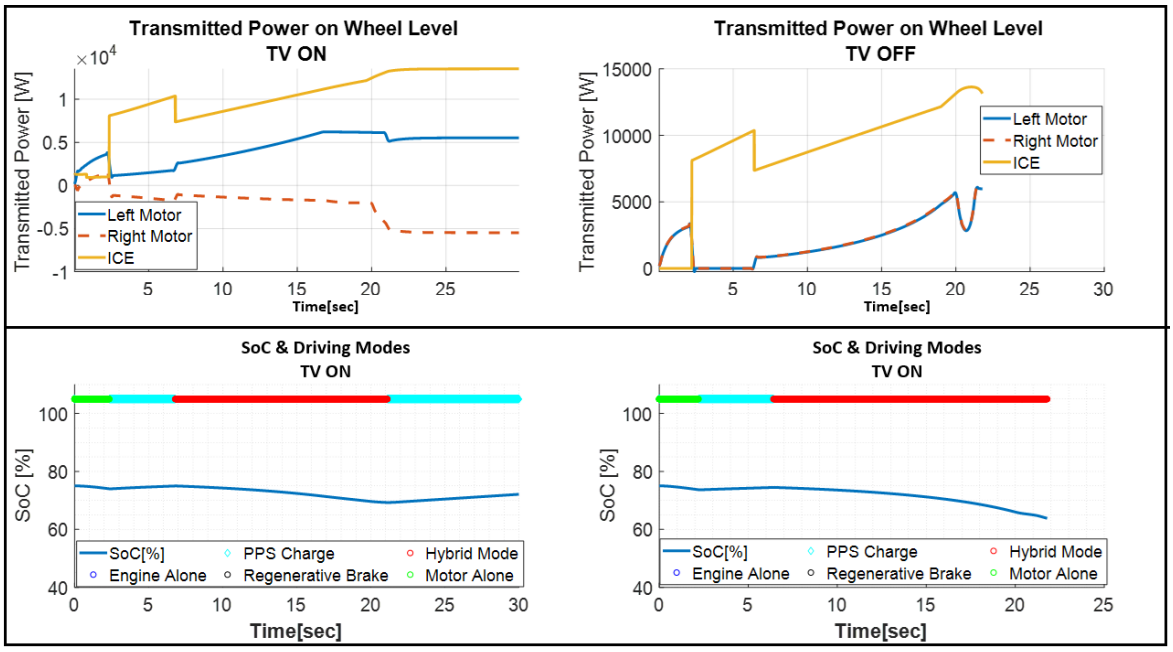

Figure 59: Transmitted Power & Battery Level

4.3.4. Test Maneuver – 4

Test Maneuver – 4 is designed to compare the effect of SoC level relative to the base model. Parameters of Test Maneuver – 4 are shown below. Not that minimum SoC level is increased from 60 to 70 and other variables are kept the same.

Table 11: Test Maneuver – 4 Parameters

Initial Longitudinal Speed $[m/s]$	10
Maximum Longitudinal Speed$[m/s\ ]$	25
Acceleration $[m/s^2\ ]$	0.75
Steer Input[degree]	25
Friction Coefficient	1
[Initial,Min,Max] SoC	75,70,90

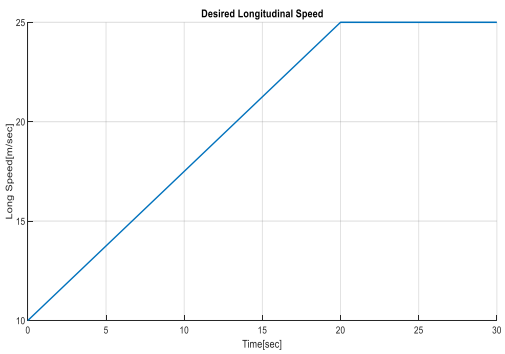

4.3.4.1. Result

The power requirement of the vehicle, which accelerates continuously during the maneuver, also increased. In previous cases, the hybrid vehicle's ICE produced power by operating on its efficient operating line, and when more power was needed, the remaining power requirement was supplied from the battery without any restriction. However, in this case, the minimum acceptable battery level was raised to 70% in this way the amount of power that can be drawn from the battery was limited.

It can be seen in Figure 62, when the battery level drops below 70%, EMS changed the "Hybrid Mode" to "PPS Charge Mode". ICE, working at full capacity, provided the power requirement of the vehicle until the battery level exceeded 70% and recharged the battery with excessive power. As the battery passed the 70% level again, EMS changed the "PPS Charge Mode" to "Hybrid Mode", and then the ICE started to work efficiently and get help from electric motors. This cycle was repeated at high frequency throughout the analysis after its start and caused front-rear torque vectoring many times, so it was a good example to examine the effect of EMS on lateral dynamics and its compatibility with DYC.

Firstly, thanks to DYC, the hybrid vehicle with TV was able to reach top speed and remain stable, albeit with a few seconds delay (Figure 60). Moreover, compared to Maneuver-3 for the same longitudinal velocities, the yaw response, side slip angle, and lateral velocity responses are quite close. This is because DYC continued to operate regardless of the battery level (Figure 62).

Another observation is that, in the hybrid vehicle, an increase in yaw velocity occurred when the “Hybrid Mode” was switched to “PPS Charge Mode”. However, during the simulation, the conventional vehicle became unstable faster because the hybrid vehicle did not accelerate as much as the conventional vehicle.

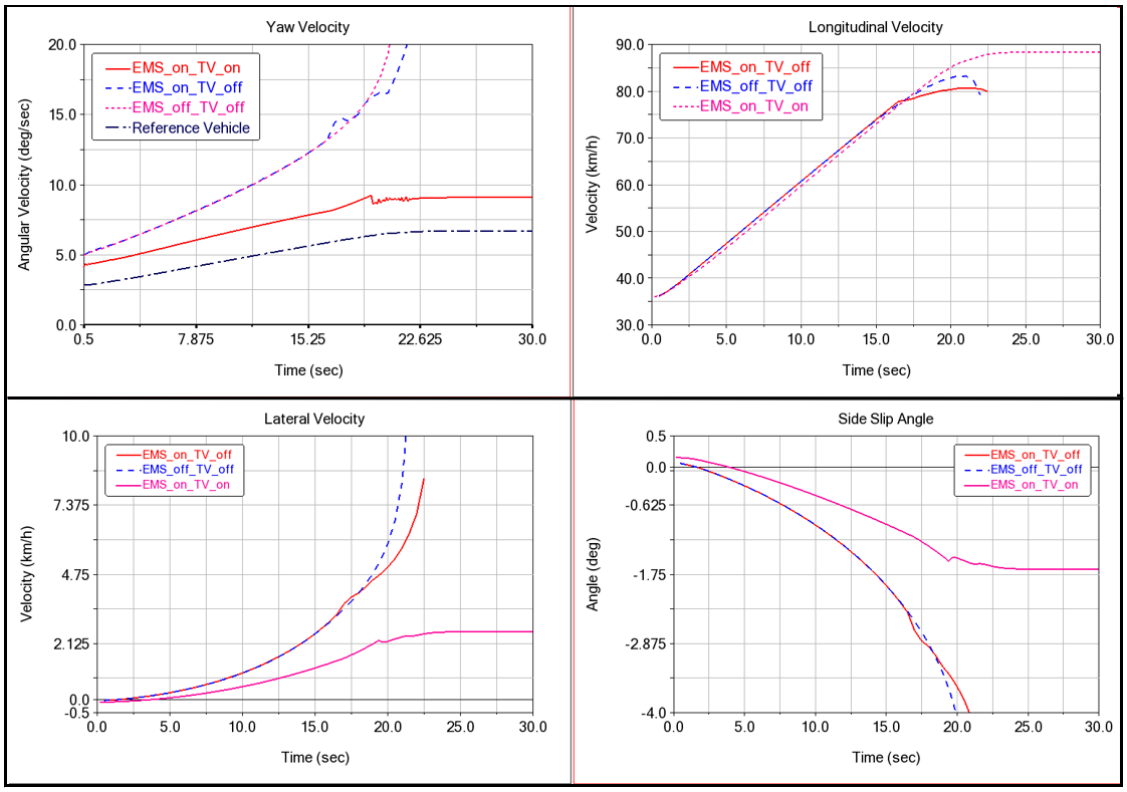

Figure 60: Vehicle Response

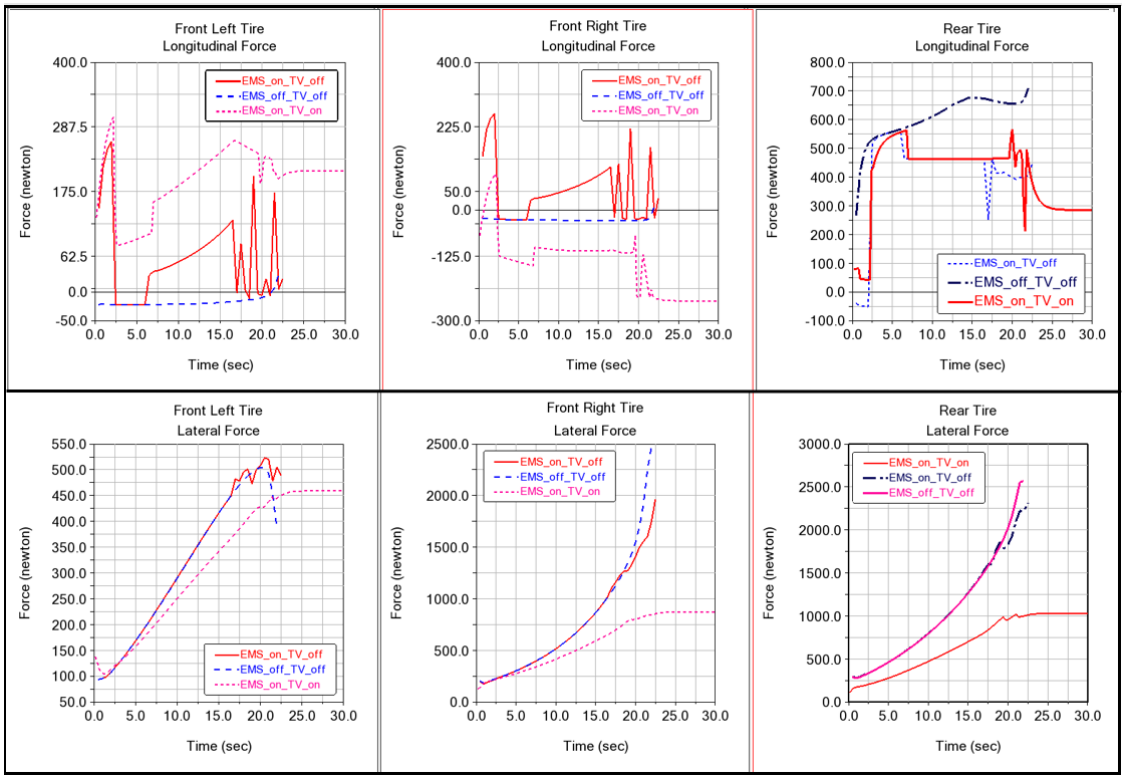

Figure 61: Tire Force

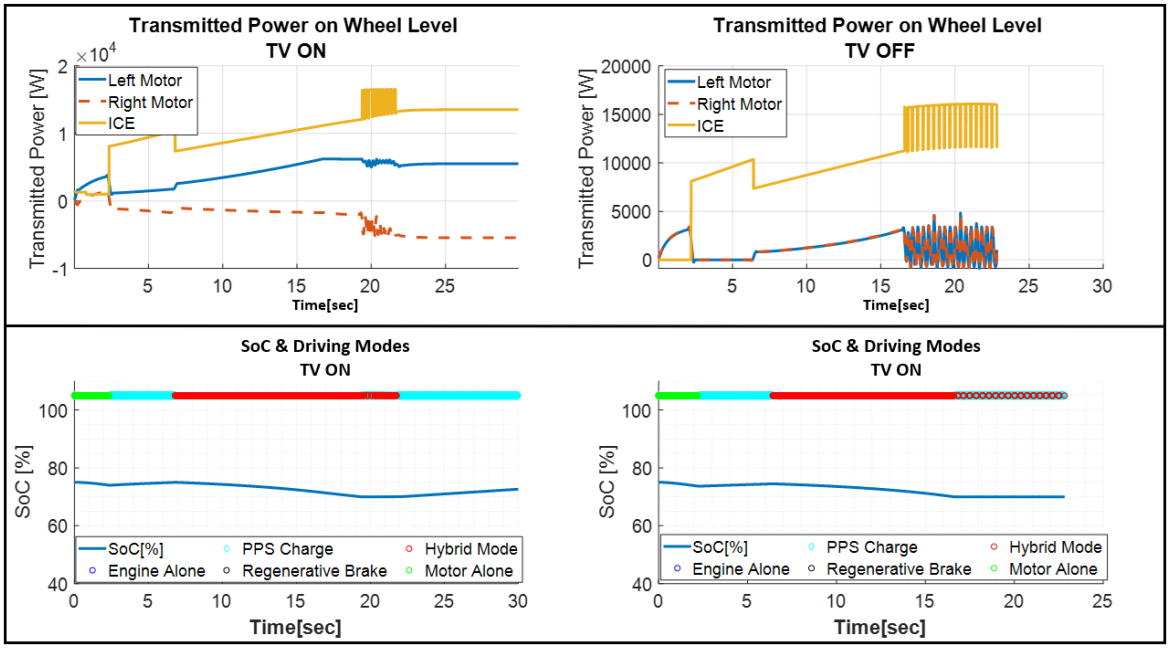

Figure 62: Transmitted Power & Battery Level

4.3.5. Test Maneuver – 5

Test Maneuver – 5 is designed to compare the effect of surface friction on lateral dynamics of the hybrid vehicle with DYC. Parameters of Test Maneuver – 5 are given below.

Table 12: Test Maneuver – 5 Parameters

Initial Longitudinal Speed $[m/s]$	10
Maximum Longitudinal Speed$[m/s\ ]$	20
Acceleration $[m/s^2\ ]$	0.5
Maximum Steer Input[degree]	25
Friction Coefficient	[1,0.75,0.5,0.2]
[Initial,Min,Max] SoC	75,60,90

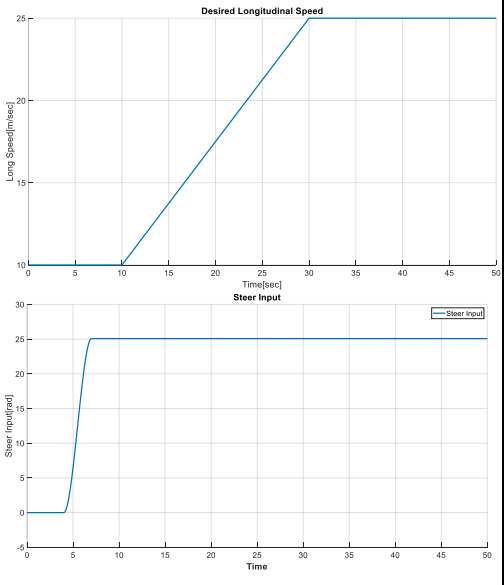

4.3.5.1. Result

The decrease in the friction coefficient causes the reduction of the maximum force that the tires can create, that is, the narrowing of the friction ellipse. This situation, which causes the tires to reach their limits earlier than expected, in other words, oversteer tendency increases with decreasing friction. However, as seen in Figure 63, even if the friction coefficient was reduced to 0.5 thanks to DYC, there were no major changes in the vehicle handling characteristics. In the case where the friction coefficient was reduced to 0.2, the stability of the vehicle was preserved, but there was an increase in its lateral velocity.

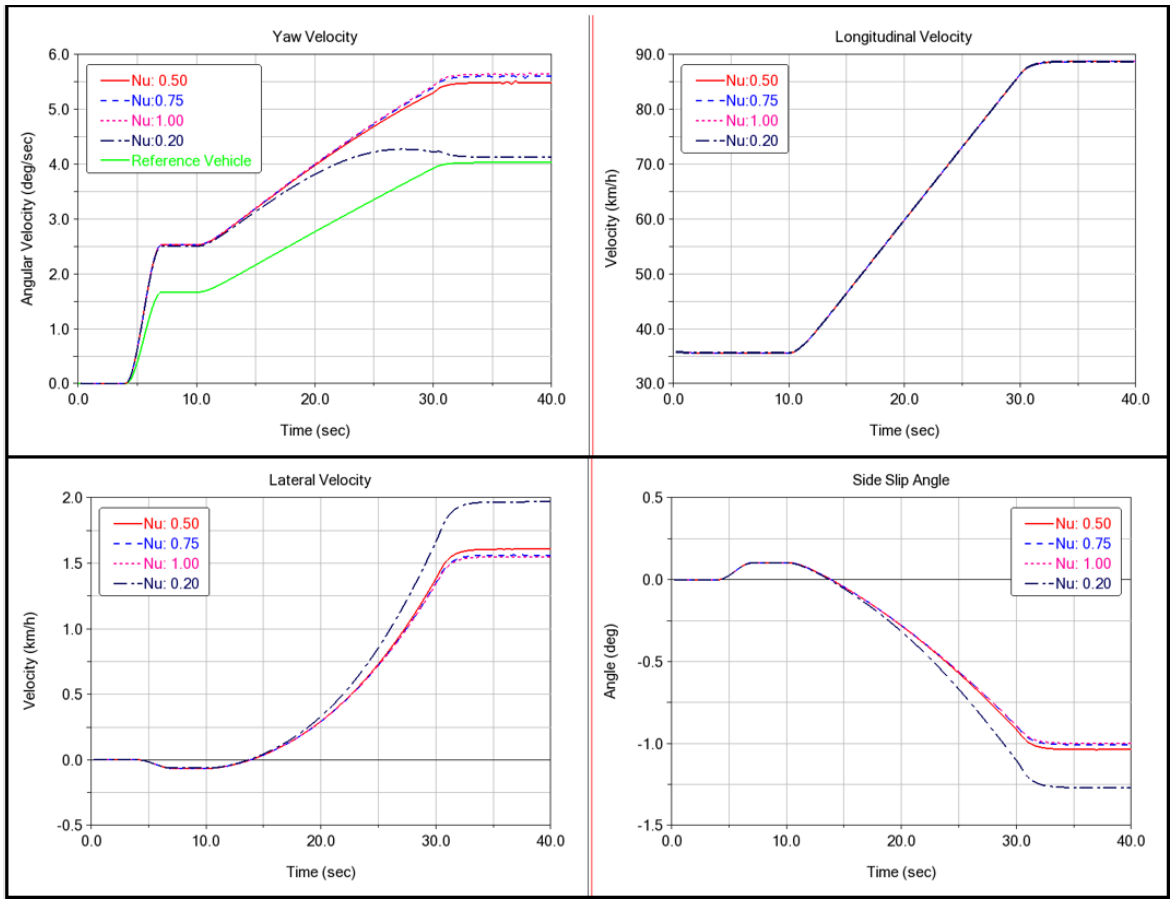

Figure 63: Vehicle Response

5. CONCLUDING REMARKS AND RECOMMENDATIONS

In this thesis, the lateral dynamics of the three-wheeled hybrid vehicle and how EMS and DYC affect the lateral characteristic were evaluated. The important step of this thesis are summarized below.

- 4 DOF nonlinear vehicle model and 2 DOF linear vehicle model were created for dynamic analysis and controller design processes.
- The vehicle model was created in Adams Car software, which succeeded in capturing the dynamic behavior of highly nonlinear problems such as large displacement and contact interactions.
- Parallel hybrid electric powertrain designed and modeled in Matlab/Simulink environment, and how the components are sized is explained.
- The energy management system is designed according to the minimum SoC strategy. The performance of the controller was examined with the UDDS drive cycle.
- Direct yaw controller with torque vectoring and active braking is designed according to the LQR control strategy. The performance of the controller was evaluated by handling analysis.
- The effects of DYC and EMS on lateral dynamics were examined and compared for different speeds, acceleration, battery level, and road friction coefficient.

5.1. Conclusion

The main conclusions of this work are summarized below:

- Thanks to the efficient use of ICE and regenerative braking, it was determined that 30% of fuel efficiency can be achieved without sacrificing longitudinal performance.
- It was observed that DYC can change the lateral behavior of the vehicle according to the specified understeer coefficient, thus increasing the handling quality and protecting the vehicle from being unstable.

- According to the analysis results with the inputs of average acceleration and average top speed, it was seen that the yaw and lateral responses of the vehicles were the same when the hybrid vehicle and conventional vehicle were compared.
- In the analysis results in which the acceleration was increased, small differences were observed due to the different longitudinal performance of the vehicle. However, when the results were examined in detail, it was understood that the almost same lateral and yaw responses were obtained for the same longitudinal velocities of hybrid and conventional vehicle.
- When the top speed was increased, both hybrid and conventional vehicles were not stable. Since some of the traction is provided by the front wheels, the hybrid vehicle's spinning started a little later than the conventional vehicle. However, it is obvious that the difference is insignificant. On the other hand, DYC kept the vehicle stable under the same conditions and ensured the completion of the test maneuver.
- It is observed that the situation in which the hybrid vehicle has to switch from "Hybrid Mode" to "PPS Charge" mode due to low battery level is the most critical in terms of lateral stability. In this case, front-to-rear torque transfer by EMS caused a sudden increase in the vehicle's yaw and lateral speed response. Fortunately, loss of speed in the vehicle caused by the sudden disabling of the electric motors prevented the vehicle from spinning. However, this behavior, which may panic the driver, is likely to cause crushes. When the situation in which the DYC was used was examined, it was observed that the lateral behavior of the vehicle was little affected, and the stability of the vehicle was preserved.
- Finally, it was observed that the performance of DYC on the low friction road decreased but continued to keep the vehicle stable.

5.2. Recommendations for Future Works

Suggestions that can be a source for future studies are as follows.

- Different control methods such as PID controller, or H_∞ can be applied for DYC.
- Different control strategies such as constraint engine on-off control strategy, fuzzy logic control technique or dynamic control technique can be applied for EMS.

- Different environmental disturbance such as nu split, side wind, grade can be included in the analysis.
- Active steering can be included in DYC.
- Other studies related to yaw and roll control, such as active cambering or tilting, can be included in the model.

- **REFERENCES**

[1] A. Zandieh, *Dynamics of a Three_Wheel Vehicle with Tadpole Design (Master's thesis, University of Waterloo),* 2005.

[2] Chatterjee, Mayurika, Kale, Mangesh, Chaudhari and Bhalchandra, "A dynamic stability control for electric narrow tilting three wheeled vehicle using integrated multivariable controller," *Transportation research part D: transport and environment,* vol. 66, pp. 58-75, 2019.

[3] Berote, Johan, Van Poelgeest, Auguste, Darling, Jocelyn, Edge, Kevin A, Plummer and Andrew, "The dynamics of a three-wheeled narrow-track tilting vehicle," in *FISITA World Automotive Congress 2008*, 2008.

[4] Claveau, Fabien, Chevrel, Mourad and Lama, "Non-linear control of a narrow tilting vehicle," in *2014 IEEE International Conference on Systems, Man, and Cybernetics (SMC)*, 2014.

[5] S. Zheng, H. Tang, Z. Han and Y. Zhang, "Controller design for vehicle stability enhancement," *Control Engineering Practice,* vol. 14, no. 12, pp. 1413-1421, 2006.

[6] G. Tekin and S. Unlusoy, "Design and simulation of an integrated active yaw control system for road vehicles," *International Journal of Vehicle Design,* pp. 5-19, 2010.

[7] E. ESMAILZADEH, G. R. VOSSOUGHI and A. GOODARZI, "Dynamic Modeling and Analysis of a Four Motorized Wheels Electric Vehicle," *Vehicle System Dynamics,* vol. 35, pp. 163-194, 2001.

[8] K. BAYAR, J. WANG and G. RIZZONI, "Development of a vehicle stability control strategy for a hybrid electric vehicle equipped with axle motors," *Proceedings of the Institution of Mechanical Engineers, Part D: Journal of automobile engineering,* pp. 795-814, 2012.

[9] T. D. GILLESPIE, Fundamentals of Vehicle Dynamics, SAE International, 1992.

[10] H. B. Pacejka, Tire and Vehicle Dynamics, SAE International, 2005.

[11] E. V. O. J. KUIPER and J. J. M. VAN OOSTEN, "The PAC2002 advanced handling tire model," *Vehicle System Dynamics,* vol. 45, pp. 153-167, 2007.

[12] J. Y. Wong, Theory of Ground Vehicles, Hoboken, NJ: Wiley, 2008.

[13] W. Bergman, "Measurement and Subjective," SAE, Destroit, 1973.

[14] H.-P. Krüger and A. Neukum, "A Workload Approach to the Evaluation of Vehicle Handling Characteristics," SAE 2000 World Congress, Detroit, Michigan, 2000.

[15] National Highway Traffic Safety Administration, "FMVSS No. 126 electronic stability control systems," *Office of Regulatory Analysis and Evaluation National Center for Statistics and Analysis,* 2007.

[16] Shibahata, Yasuji, Shimada, Kazuhiko, Tomari and Tatsuhiro, "Improvement of vehicle maneuverability by direct yaw moment control," *Vehicle System Dynamics,* pp. 465-481, 1993.

[17] Rieger, Gerhard and Scheef, Joachim and Becker, Holger and Stanzel, Michael and Zobel and Robert, "Active Safety Systems Change Accident Environment of Vehicles Significantly - A Challenge for Vehicle Design," *Proceedings: International Technical Conference on the Enhanced Safety of Vehicles,* pp. 11-11, 2005.

[18] Liebemann, EK and Meder, K and Schuh, J and Nenninger and G, "Safety and performance enhancement: The Bosch electronic stability control (ESP)," *SAE Technical Paper,* 2004.

[19] Aga, M. and Okada and A., "Analysis of vehicle stability control (vsc)'s effectiveness from accident data," *Proceedings: International Technical Conference on the Enhanced Safety of Vehicles,* p. 7, 2003.

[20] Farmer and M. Charles, "Effect of electronic stability control on automobile crash risk," *Traffic injury prevention,* pp. 317-325, 2004.

[21] J. Kiumars, *Stability Control of Electric Vehicles with In-wheel Motors,* UWSpace, 2010.

[22] Grogg, John and Yuan, Qinghui and Lew and Jae, "Dynamic Modeling of Torque-Biasing Devices for Vehicle Yaw Control," *SAE International,* pp. 14-16, 2006.

[23] Piyabongkarn, Damrongrit and Rajamani, Rajesh and Lew, Jae Y and Yu and Hai, "On the use of torque-biasing devices for vehicle stability control," in *American Control Conference*, 2006.

[24] Ghosh, Jyotishman and Tonoli, Andrea and Amati and Nicola, "A torque vectoring strategy for improving the performance of a rear wheel drive electric vehicle," in *2015 IEEE Vehicle Power and Propulsion Conference (VPPC)*, 2015.

[25] A. Saeedi and R. Kazemi, *Stability of Three-Wheeled Vehicles with and without Control System,* International Journal of Automotive Engineering, 2013.

[26] Wheals, Jonathan C and Baker, Hanna and Ramsey, Keith and Turner and Will, "Torque vectoring AWD driveline: design, simulation, capabilities and control," *SAE transactions,* pp. 557-576, 2004.

[27] International Energy Agency, 2018. [Online]. Available: https://www.iea.org.

[28] EEA (European Environment Agency) Report, "Trends and projections inEurope 2013: Tracking progress towards Europe's climate and energy targetsuntil 2020," 2013.

[29] Y. Hori, "Future vehicle driven by electricity and control-research on four wheel motored "UOT Electric March II"," in *7th International Workshop on Advanced Motion Control. Proceedings (Cat. No.02TH8623)*, 2002, pp. 1-14.

[30] Chau, KT and Wong and YS, "Overview of power management in hybrid electric vehicles," *Energy conversion and management,* vol. 43, pp. 1953-1968, 2002.

[31] B. R. Munson, A. P. Rothmayer, T. H. Okiishi and W. W. Huebsch, Fundamentals of Fluid Mechanics, 7th ed., Wiley, 2012.

[32] G. Yimin, R. M. Khwaja and E. Mehrdad, "Parametric Design of Drive Train of an Electrically Peaking Hybrid (ELPH) Vehicle," *970294,* 1997.

[33] M. Ehsani, Y. Gao, S. Longo and K. M. Ebrahimi, Modern Electric, Hybrid Electric, and Fuel Cell Vehicles, CRC Press, 2018.

[34] M. Ehsani, K. M. Rahman and H. A. Toliyat, "Propulsion system design of electric and hybrid vehicle," *IEEE Trans. Ind. Electron.,* 1997.

[35] T. Hofman, M. Steinbuch, R. van Druten and A. Serrarens, "Rule Based energy management strategies for hybrid vehicles," *Int. J. Electric and,* pp. 71-94, 2007.

[36] K. Ettihir, L. Boulon and K. Agbossou, "Optimization-based energy management strategy for a fuel cell/battery hybrid power system," *Applied Energy,* pp. 142-153, 2016.

[37] "EPA Emission Standards for Light-Duty Vehicles and Trucks and Motorcycles," [Online]. Available: https://www.epa.gov/emission-standards-reference-guide/epa-emission-standards-light-duty-vehicles-and-trucks-and.

[38] *ADAMS/Tire Manual,* Corporation, MSC Software, 2005.

[39] R. B. GmbH, Driving-safety Systems, R. B. GmbH., Ed., Bosch, 1999.